Functional Analysis of Calmodulin's Calcium Dependent Inactivation of Orai1

by Drake Jensen, Bachelor of Arts and Science

A Thesis Submitted in Partial
Fulfillment of the Requirements
for the Degree of
Master of Science
in the field of Chemistry

Advisory Committee:

Chin-Chuan Wei, Chair

Leah O'Brien

Tom Fowler

Graduate School
Southern Illinois University Edwardsville
May, 2015

ABSTRACT

FUNCTIONAL ANALYSIS OF CALMODULIN'S CALCIUM DEPENDENT INACTIVATION OF ORAI1

by

DRAKE JENSEN

Chairperson: Chin-Chuan Wei

Calmodulin (CaM) plays an important role in calcium (Ca^{2+})-dependent signal transduction. Ca^{2+} binding to CaM triggers a conformational change, forming a hydrophobic patch that is important for target protein recognition. CaM regulates a Ca^{2+}-dependent inactivation (CDI) process in store-operated Ca^{2+} entry (SOCE), by interacting with the N-terminus of the hexameric plasma membrane Ca^{2+} channel Orai1. To understand the relationship between Ca^{2+}-induced hydrophobicity of CaM and the CaM/Orai interaction, chimeric proteins constructed by exchanging EF-hands of CaM with those of Troponin C (TnC) were used as an informative probe to better understand the functionality of each EF-hand.

1-Anilinonaphthalene-8-Sulfonic acid (ANS) was used to assess the context of the induced hydrophobic surface on CaM and chimeras upon Ca^{2+} binding. The exchanged EF-hands from TnC to CaM resulted in reduced hydrophobicity compared with wild-type CaM, as depicted by ANS fluorescence and binding affinity. Such a conclusion is consistent with general concepts about the inadequacy of hydrophobic exposure for chimeras. However, these ANS responses exhibited no correlation with the ability to interact with

Orai1. ANS lifetime measurements indicated that there are two types of ANS molecules with rather distinct fluorescence lifetimes, each specifically corresponding to one lobe of CaM or chimeras. Thermodynamic studies indicated the interaction between CaM and a 24-residue peptide corresponding to the CaM-binding domain of Orail1 (Orai-CMBD) is a 1:2 CaM/Orai-CMBD binding, in which the binding of each peptide yields a similar enthalpy change ($\Delta H = -5.02 \pm 0.13$ kcal/mol) and binding affinity ($K_a = 8.92 \pm 1.03 \times 10^5\ M^{-1}$). Chimeras noted as CaM(1TnC) and CaM(2TnC), with exchanged EF1 and EF2, displayed a two-sequential binding mode with a one-order weaker binding affinity and lower ΔH than that of CaM, while CaM(3TnC) and CaM(4TnC) had similar binding thermodynamics as CaM. Circular Dichroism studies suggested differences in binding most likely resulted from changes in chimera three-dimensional structure rather than secondary structure, as the extent of α-helical content from apo-, Ca^{2+}-, and Orai-CMBD-bound proteins remained similar. The dissociation rate constant for CaM/Orai-CMBD was determined to be $1.41 \pm 0.08\ s^{-1}$ by rapid kinetics. Stern-Volmer plots of Orai-CMBD Trp76 indicated that the residue is located in a very hydrophobic environment but became more solvent accessible when EF1 and EF2 were exchanged. Here, the model of 1:2 binding stoichiometry of CaM/Orai-CMBD established in solution supports the unique, open binding mode suggested by published structural studies.

ACKNOWLEDGEMENTS

I would like to thank the members of my thesis committee: Drs. Wei, O'Brien, and Fowler. First and foremost, I would like to extend my deepest gratitude to Dr. Chin-Chuan Wei. When I joined the Wei lab back in April 2012 as an undergraduate student, I was warned by my peers that due to the high expectations, I would not have a life outside of the lab. While that may have been partially true, three years later I've realized that I want my life to be driven by scientific pursuits (albeit with a few extra-curricular activities here and there to keep me sane). Under Dr. Wei's guidance, such pursuits became apparent, as the decision to continue on for a PhD is now more than obvious. Being provided with hands-on training while working alongside Dr. Wei, I gained invaluable expertise in both standard lab protocols and state of the art instrumentation. Dr. Wei often allowed me to conduct experiments outside of my thesis work, better preparing me for the research I will encounter as a PhD student. He has devoted an enormous time to ensure my success, and for that I am extremely grateful.

Second, I would like to extend my thanks to Dr. Leah O'Brien. Having been provided with the opportunity to teach alongside of Dr. O'Brien in classes that she instructed me in as an undergraduate, has helped immensely in developing my own teaching pedagogy. In developing a close, professional relationship over the years, I have come to regard her as a second mentor, and have greatly come to value her professional advice.

Finally, I would like to thank Dr. Tom Fowler. Having had him as an instructor for Genetics and Recombinant DNA lecture and lab courses instilled a firm knowledge of both the theory and practice behind many experimental techniques needed for biological research. As I look ahead to my PhD where I plan to pursue biophysical approaches in molecular genetics, the expertise that I have acquired from his teaching will prove invaluable.

In addition to my thesis committee members, I would like to extend a special thanks to Dr. Shaw in the chemistry department and Dr. Liebl in the biology department, both of which have taken a great interest in my career at SIUE and aided immensely in my professional development.

I am also grateful for the department of chemistry and their continued support of education and research. The department has graciously funded my travel to three national conferences, where I was able to present my thesis work and other ongoing projects.

I would be hard-pressed not to thank my family, specifically my parents, for both their emotional and financial support during my years at SIUE. My parents have perhaps played the most instrumental role in my success, instilling hard-working values and demonstrating the importance of an education from a young age.

In terms of the thesis research performed, there are many that are deserving of thanks. My past lab members Katie Bennett, Nicole Reynolds, and Allison Tatro were instrumental in providing the necessary training in protein expression/purification techniques. Shubha Shakya got this project up and running, as she collected some of the preliminary CaM/Orai1 data prior to her graduation in 2013. Kyle Schaffer and Dallas Wright (current lab members) deserve credit for their additional help in protein purification. I would like to extend a special thanks to Dr. Carl Frieden at Washington University in St. Louis for allowing us to use his CD spectrometer, Dr. Samuel E. George at Duke University for providing us with the plasmid constructs for the chimera proteins, and Dr. Lutz Birnbaumer at NIH for providing us with the three-dimensional coordinates of the CaM/Orai-CMBD crystal structure and the hypothetical N-terminal CaM/Orai-CMBD interaction.

I would also like to thank the internal financial support obtained from Southern Illinois University Edwardsville: Seed Grants for Transitional and Exploratory Projects

(STEP), Research Grants for Graduate Students (RGGS) and Undergraduate Research and Creative Activities (URCA) Associate Awards. This work was supported in part by Cottrell College Science Awards 7322 from Research Corporation and National Science Foundation grant DUE-0941517 to Chin-Chuan Wei.

TABLE OF CONTENTS

ABSTRACT……..ii

ACKNOWLEDGEMENTS……..iv

LIST OF FIGURES…….....x

LIST OF TABLES……....xi

LIST OF EQUATIONS……..….xii

LIST OF ABBREVIATIONS……xiii

Chapter

1 INTRODUCTION……...1

1.1 Physiological Calcium Signaling……1

1.2 Store Operated Calcium Entry……...…5

1.3 Physiological Significance of SOCE……...…….....14

1.4 EF-Hand Superfamily and Its Members: Calmodulin and Troponin C……...…….15

1.5 Statement of Purpose……...……...……...22

2 EXPERIMENTAL…….....24

2.1 General…….24

2.2 Recombinant Protein Expression/Purification…….....24

2.2.1 Transformation of plasmid DNA to obtain glycerol cell stocks……...…25

2.2.2 Recombinant protein expression…….....26

2.2.2.1 CaM and CaM(3TnC)……...……..26

2.2.2.2 CaM(1TnC), CaM(2TnC), and CaM(4TnC)……...…...27

2.2.3 Cell lysis and protein extraction……..27

2.2.4 Recombinant protein purification……...28

2.2.4.1 CaM, CaM(1TnC), CaM(2TnC), and CaM(4TnC)……..…..28

2.2.4.2 CaM(3TnC)……..……..28

2.3 Preparation of Ca^{2+}-Free Proteins……....29

2.4 Determination of Protein Concentration and Purity……....29

2.5 Dansyl Chloride Labeling……....30

2.6 Isothermal Titration Calorimetry…….30

2.7 Spectroscopic Measurements……..…….31

2.8 Stern-Volmer Quenching……..…...33

2.9 Far-UV Circular Dichroism (CD)……...….34

2.10 Modeling…….....35

3 RESULTS AND DISCUSSION…….…….....36

3.1 Structual Change of CaM and Chimeras Probed with ANS……...36

3.2 Fluorescence Studies Reveal the Ca^{2+}-Dependent Interaction between Orai Peptide and CaM Derivatives……..……...…43

3.3 Stern-Volmer Quenching to Determine the Solvent Accessibilty of Trp 76…..….46

3.4 Thermodynamics of Orai-CMBD to CaM and Chimeras……....48

3.5 Kinetics of Orai-CMBD to CaM and Chimeras……..51

3.6 Circular Dichroism to Monitor Secondary Structure Changes…….....54

3.7 Modeling and Solvent Accessible Calculations……..……56

3.8 Rationale of Experimental Data with the Existing Structual Information of CaM/Orai-CMBD…….……..……..58

4 CONCLUSIONS……………………………………………………………………...63

REFERENCES………………………………………………………………………67

LIST OF FIGURES

Figure 1 : Intracellular Ca^{2+} signaling on and off reactions..... 2

Figure 2 : Ca^{2+} signaling mediated by channles, pumps and protein effectors..... 4

Figure 3 : Store operated Ca^{2+} entry signaling.…..... 7

Figure 4 : Diagram of the STIM1/Orai1 complex and key domains 9

Figure 5 : EF-hand motif structure and ligand coordination for Ca^{2+} chelation 16

Figure 6 : Apo- and Ca^{2+}-bound CaM structures and target interactions. 19

Figure 7 : Sequence alignment of hCaM, cTnC and chimeras. 22

Figure 8 : ANS fluorescence of uncomplexed and complexed CaM and CaM(3TnC) 37

Figure 9 : ANS binding to CaM and CaM(3TnC) by isothermal titration calorimetry 39

Figure 10 : The lifetime measurement of CaM-bound ANS 41

Figure 11 : Trp76 Orai-CMBD fluorescence of CaM and CaM(2TnC). 44

Figure 12 : Stern-Volmer plot of Trp76 fluorescence of Orai-CMBD quenched by acrylamide 47

Figure 13 : The binding thermodynamics of Orai-CMBD to CaM and CaM(1TnC) determined by ITC..... 51

Figure 14 : Kinetics of Orai-CMBD to CaM and chimeras..... 53

Figure 15 : Circular Dichroism spectra of Orai-CMBD alone and complexed with CaM 55

Figure 16 : The proposed model of the 1:2 CaM/Orai-CMBD complex..... 60

Figure 17 : The hypothetical interaction of Orai-CMBD to CaM-N and CaM-C 62

LIST OF TABLES

Table 1 : ANS binding to CaM and chimeras by fluorescence and ITC 39

Table 2 : ANS lifetime for the uncomplexed and complexed CaM and chimeras 42

Table 3 : Trp76 of Orai-CMBD fluorescence and Stern-Volmer quenching constants 48

Table 4 : Thermodynamics and kinetics of Orai-CMBD to CaM and chimeras 53

Table 5 : Ellipticity ratios for apo-, Ca^{2+}-, and Orai-CMBD-bound CaM and chimeras 56

LIST OF EQUATIONS

Equation 1 : Isothermal titration calorimetry buffer protonation/ionization 31

Equation 2 : Lifetime fluorescence intensity, fractional intenisty and pre-exponential factors…….……..…..32

Equation 3 : Stopped-flow kinetics dissociation……..33

Equation 4 : Steady-state Stern-Volmer quenching……..……...…34

Equation 5 : Lifetime Stern-Volmer quenching……...34

LIST OF ABBREVIATIONS

Ala	Three letter abbreviation for alanine amino acid residue
Amp	Ampicillin
ANS	1-Anilinonaphthalene-8-Sulfonic acid
APBS	Adaptive Poisson-Boltzmann solver
Apo	Without bound ligand
ASA	Accessible surface area
ASA_{ap}	Apolar accessible surface area
ASA_{p}	Polar accessible surface area
Asp	Three letter abbreviation for aspartate amino acid residue
BSA	Bovine serum albumin
CA	Ca^{2+}-ATPase
Ca^{2+}	Calcium
CaBP	Ca^{2+} binding proteins
CAD	CRAC activation domain
CaM	Calmodulin
CaM-C	C-terminal lobe of Calmodulin
CaM-N	N-terminal lobe of Calmodulin
CaMKII	Calmodulin dependent protein kinase II
CaMKIV	Calmodulin dependent protein kinase IV
CaM(1TnC)	Chimera protein with 1^{st} EF-hand of TnC and 2^{nd}, 3^{rd}, and 4^{th} EF-hand of CaM
CaM(2TnC)	Chimera protein with 2^{nd} EF-hand of TnC and 1^{st}, 3^{rd}, and 4^{th} EF-hand of CaM
CaM(3TnC)	Chimera protein with 3^{rd} EF-hand of TnC and 1^{st}, 2^{nd}, and 4^{th} EF-hand of CaM
CaM(4TnC)	Chimera protein with 4^{th} EF-hand of TnC and 1^{st}, 2^{nd}, and 3^{rd} EF-hand of CaM

Ca_V 1.2	Calcium channel, voltage-dependent, L type, alpha 1C subunit
CD	Circular Dichroism
CDI	Ca^{2+}-dependent inactivation
cDNA	Complementary DNA
CMBD	CaM-binding domain
CMD	CRAC modulatory domain
CRAC	Ca^{2+} release-activated Ca^{2+}
CRACM1	CRAC modulator 1
CRACR2A	CRAC regulator 2A
CREB	cAMP response element-binding protein
CT	Charge transfer
CTID	C-terminal inhibitory domain
cTnC	Cardiac Troponin C
D	One letter notation for aspartate amino acid residue
DAG	Diacylglycerol
DMF	Dimethyl formamide
E	One letter notation for glutamate amino acid residue
E. coli	*Escherichia coli*
EDTA	Ethylenediaminetetraacetic acid
EF	EF-hand domain
ER	Endoplasmic reticulum
F	One letter notation for phenylalanine amino acid residue
FADD	Fas-associated death domain
FPLC	Fast protein liquid chromatography

FRET	Fluorescence resonance energy transfer
GPCR	G-protein coupled receptor
Glu	Three letter abbreviation for glutamate amino acid residue
hCaM	human Calmodulin
HEPES	(4-(2-hydroxyethyl)-1-piperazineethanesulfonic acid)
HIC	Hydrophobic interaction chromatography
His_6	Six histidine tag
I	One letter notation for isoleucine amino acid residue
I_{CRAC}	CRAC current
IgE	Immunoglobulin E
Ile	Three letter abbreviation for isoleucine amino acid residue
IP_3	Inositol trisphosphate
IP_3R	Inositol triphosphate receptor
IPTG	Isopropyl-β-D-1-thiogalactopyronoside
IQ	Isoleucine-glutamine binding motif
ITC	Isothermal titration calorimetry
K^+	Potassium
KI	Potassium Iodide
L	One letter notation for leucine amino acid residue
LB	Luria broth
Leu	Three letter abbreviation for leucine amino acid residue
M	One letter notation for methionine amino acid residue
MWCO	Molecular weight cut off
M13	Skeletal Muscle Myosin Light Chain Kinase Peptide (SK - MLCK M13)

NaCl	Sodium chloride
NADDP	Nicotinic acid adenine dinucleotide phosphate
NCX	Na^+/Ca^{2+} exchanger
NFAT	Nuclear factor of activated T cells
Ni-NTA	Nickel-nitrilotriacetic acid
NMR	Nuclear magnetic resonance
NMR NOE	Nuclear magnetic resonance nuclear overhauser effect
NOS	Nitric Oxide Synthase
nNOS	Neuronal Nitric Oxide Synthase
OD	Optical density
PDB	Protein data bank
Phe	Three letter abbreviation for phenylalanine amino acid residue
PIP_2	Phosphatidylinositol 4,5-bisphosphate
PLC-β	Phospholipase C-β
PLC-γ	Phospholipase C-γ
PM	Plasma membrane
PMCA	Plasma membrane Ca^{2+}-ATPase
POPS	Piperazine-N,N-bis(2-hydroxypropanesulfonic acid)
Q	One letter notation for glutamine amino acid residue
R	One letter notation for arginine amino acid residue
RMSD	Root mean square deviation
RNAi	RNA interference
ROC	Receptor-operated channels
rpm	Revolutions per minute

RYR	Ryanodine receptor
S	One letter notation for serine amino acid residue
SAM	Sterile alpha motif
SARAF	SOCE-associated regulatory factor
SCID	Severe combined immunodeficiency
SDS-PAGE	Sodium dodecyl sulfate-polyacrylamide gel electrophoresis
SERCA	Sarcoplasmic reticulum/endoplasmic reticulum Ca^{2+} ATPase
smMLCK	Smooth muscle myosin light chain kinase
SMOC	Second messenger-operated channels
SOAR	STIM1 Orai activating region
SOCE	Store-operated Ca^{2+} entry
SOC	Store-operated channels
SOC medium	Super optimal broth with catabolite repression growth media
SR	Sarcoplasmic reticulum
STIM1	Stromal interaction molecule 1
STIM2	Stromal interaction molecule 2
sTnC	Skeletal Troponin C
T	One letter notation for threonine amino acid residue
TCSPC	Time-correlated single photon counting
Thr	Three letter abbreviation for threonine amino acid residue
TM	Transmembrane
TnC	Troponin C
TNS	2-p-Toluidinyl-naphthalene-6-sulfonate
Tris	Tris(hydroxymethyl)aminomethane

Trp	Three letter abbreviation for tryptophan amino acid residue
TRP	Transient receptor potential
TRPC	Transient receptor potential canonical
TRPC1	Transient receptor potential canonical 1
Tyr	Three letter abbreviation for tyrosine amino acid residue
UV-Vis	Ultraviolet-visible
V	One letter notation for valine amino acid residue
Val	Three letter abbreviation for valine amino acid residue
VDW	van der Waals
VOC	Voltage-operated channels
W	One letter notation for tryptophan amino acid residue
Y	One letter notation for tyrosine amino acid residue

CHAPTER 1

INTRODUCTION

1.1 Physiological Calcium Signaling

Calcium (Ca^{2+}) signaling controls virtually every aspect of cellular life including, but not limited to, cell proliferation, T cell activation, muscle contraction, vesicular fusion, exocytosis, and apoptosis. The plasma membrane (PM) and membranes of many intracellular organelles separate the cytosol, which has a low resting Ca^{2+} concentration of approximately 100 nM, from the extracellular space where the Ca^{2+} concentration remains near 5 mM (Taylor et al., 2009). When a biological event occurs, Ca^{2+} ions are free to diffuse down their electrochemical gradient, both passively and actively, and the regulated opening of Ca^{2+} channels means that most intracellular and extracellular signals will cause a sudden increase in cytosolic Ca^{2+} concentrations to approximately 1 μM (Bootman, 2012). Ca^{2+} channel proteins that mediate such an activity include: 1) voltage operated channels (VOCs), which are activated by membrane depolarization; 2) second messenger-operated channels (SMOCs), which are typically activated by inositol phosphates, cyclic nucleotides, or lipid-derived messengers (diacylglycerol (DAG) and arachidonic acid and their associated metabolites); 3) store-operated channels (SOCs), which are activated by depletion of intracellular endoplasmic reticulum (ER) and sarcoplasmic reticulum (SR) Ca^{2+} stores; and 4) receptor-operated channels (ROCs), which are activated by direct binding of a hormonal agonist or neurotransmitter (Parekh and Putney, 2005). By the end of the biological event, the signal itself can be viewed as reversible, in that the cytosolic Ca^{2+} concentration decreases and returns to its resting state. A decrease in Ca^{2+} concentration is

accomplished by refilling the ER and SR Ca^{2+} stores and by the extrusion of Ca^{2+} via Na^{+}/Ca^{2+} exchanges (NCXs), plasma membrane Ca^{2+}-ATPases (PMCAs) and SR/ER Ca^{2+} ATPases (SERCAs). Thus Ca^{2+} signaling consists of both "on" and "off" reactions, in which cytosolic Ca^{2+} concentrations are oscillated (Figure 1).

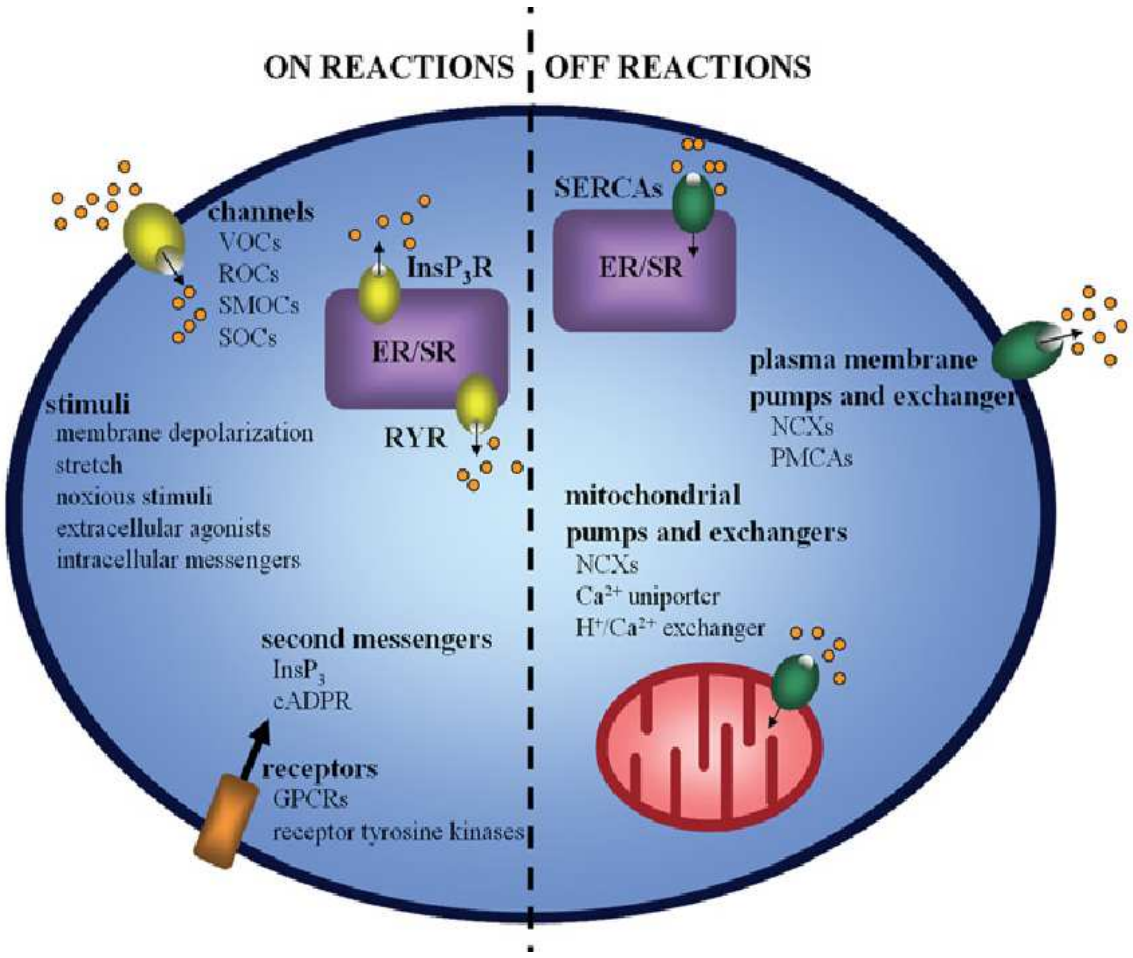

Figure 1: Intracellular Ca^{2+} signaling on and off reactions (Parekh and Putney, 2005). The competing "on" and "off" reactions are what ultimately determines the cytosolic Ca^{2+} concentration, in which passive diffusion of Ca^{2+} ions through permeable channels mediate the most rapid changes and are thus most commonly regulated by signaling pathways (Taylor et al., 2009).

Ca^{2+}-signaling is also tissue specific, in which signaling proteomes modulate signals that suit a tissue's physiological needs (Berridge et al., 2003). For example, Ca^{2+} VOCs and ROCs (which rapidly open upon external ligand binding) are found in excitable cells like nerve and muscle but are largely excluded from non-excitable cells (Parekh and Putney, 2005). Excitable myocyte cells require rapid (hundreds of milliseconds) whole cell Ca^{2+} transients for contraction to be triggered every second (Bers, 2002). These transients are generated by Ca^{2+} entry through VOCs in the PM, which then triggers Ca^{2+} release into the cytosol by ryanodine receptors (RYR) on the SR (Figure 2). Non-excitable cells have much slower Ca^{2+} oscillations (tens of seconds), thus maintaining a longer periodical time to control metabolism and gene expression (Dupont et al., 2011). The slower Ca^{2+} signals are typically mediated by the second messengers inositol trisphosphate (IP_3) and nicotinic acid adenine dinucleotide phosphate (NAADP) which bind to IP_3-Receptor channels (IP_3Rs) and NAADP-gated Ca^{2+}-two pore channels on the ER to promote increased cytosolic Ca^{2+} concentrations (Figure 2) (Galione, 2011). On the other hand, store operated Ca^{2+} permeable channels (SOCs) are found ubiquitously in all eukaryotes from humans (Partiseti et al., 1994) to yeast (Locke et al., 2000), suggesting both a primordial and necessary function in Ca^{2+} signaling and homeostasis.

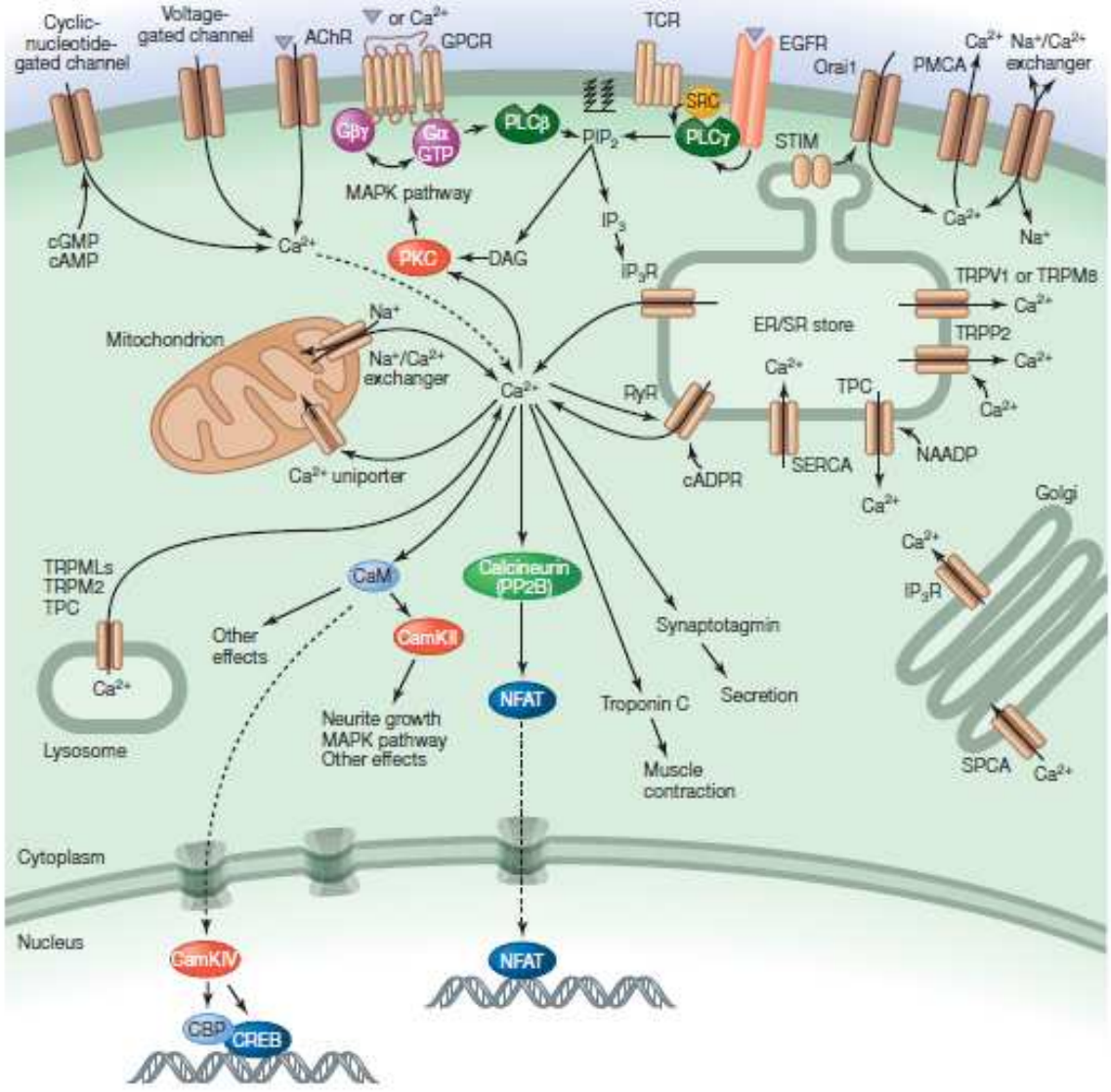

Figure 2: Ca^{2+} signaling mediated by channels, pumps and protein effectors (Bootman, 2012). Plasma membrane channels and pumps, along with organelle channels and pumps act in concert to regulate Ca^{2+} oscillations. As cytosolic Ca^{2+} concentrations increase, particular effectors (kinases, such as Calmodulin dependent kinase II and IV (CaMKII and CaMKIV); phosphatases, such as Calcineurin; transcription factors, such as CREB (cAMP response element-binding protein) and NFAT (nuclear factor of activated T-cells); and Ca^{2+}-binding proteins, such as Calmodulin (CaM) and Troponin C (TnC)) become activated to promote downstream signaling and regulation of physiological events.

1.2 Store-Operated Calcium Entry

The concept of store operated Ca^{2+} entry (SOCE) was first noted in 1986, in which it was revealed that the amount of Ca^{2+} in the ER stores determined the resultant intracellular Ca^{2+} influx, a process originally called capacitative Ca^{2+} entry in parotid acinar cells (Takemura and Putney, 1989). In addition to serving as a Ca^{2+} store, the lumenal ER also mediates protein folding/processing by Ca^{2+} dependent chaperones, vesicular trafficking (Gorelick and Shugrue, 2001), regulation of cholesterol metabolism (Brown and Goldstein, 1999), and apoptosis or programmed cell death (Ferri and Kroemer, 2001). Many of such processes require intraluminal Ca^{2+}, and upon depletion of lumenal Ca^{2+} stores, release of stress signals (Kaufman, 1999), protein misfolding, and apoptosis can be induced over prolonged periods of time (Parekh and Putney, 2005). Thus, it becomes clear that the ER lumenal Ca^{2+} concentration decreases following stimulation, and replenishment of the stores is vital for all eukaryotic cells. SOCs aid in maintaining a consistent intracellular Ca^{2+} storage concentration and can generate secondary signals to aid in gene expression, exocytosis and cell metabolism (Berridge, 2012). SOCE differs from most chemical Ca^{2+} sensing pathways given that it determines low lumenal Ca^{2+} levels, and thus any channel that can exhibit Ca^{2+}-store dependency can be termed SOC (Symth et al., 2006).

The most studied and functionally best understood SOC is the Ca^{2+} release-activated Ca^{2+} (CRAC) channel, which has been implemented in many immunological functions including T-lymphocyte activation via NFAT (Feske et al., 2005) and mast cell degranulation in response to IgE receptor-mediated signaling (Holowka et al., 2012; Wolfe et al., 1996; Vig et al., 2008). The mechanism of the CRAC channel is mediated by two protein components as determined by a genome-wide RNAi screen in *Drosophila* cell lines: Orai1 (also referred

to as CRAC modulator or CRACM1) as the PM pore forming subunit and Stromal Interaction Molecule 1 (STIM1) as the ER-resident store-sensor (Liou et al., 2005; Vig et al., 2006a; Vig et al., 2006b). As previously stated, a declining ER Ca^{2+} concentration, not an increasing cytoplasmic Ca^{2+} concentration, activates CRAC channels. This is a critical distinction that separates CRAC channels from transient receptor potential canonical (TRPC) and K^+ channels (Clapham, 2009). Briefly, a mechanism for CRAC channel activation is shown in Figure 3A (Hewavitharana et al., 2007). G-protein coupled receptors (GPCRs) or tyrosine kinase coupled receptors activate phospholipase C-β or PLC-γ resulting in breakdown of phosphatidylinositol 4,5-bisphosphate (PIP_2). The breakdown of PIP_2 releases inositol 1,4,5-trisphosphate or simply inositol triphosphate (IP_3) into the cytoplasm. Subsequent binding to the IP_3 receptor on the ER causes the release of Ca^{2+} from the ER lumen. Ca^{2+} storage depletion in the ER results in the loss of Ca^{2+} bound to STIM1, causing aggregation and migration to a region close to the plasma membrane where it interacts with Orai1 to permit Ca^{2+} influx (Figure 3B). To return to a resting cell Ca^{2+} concentration state, prompt inactivation of the Orai1 channel must occur through a process called Ca^{2+}-dependent inactivation (CDI) (Mullins et al., 2009).

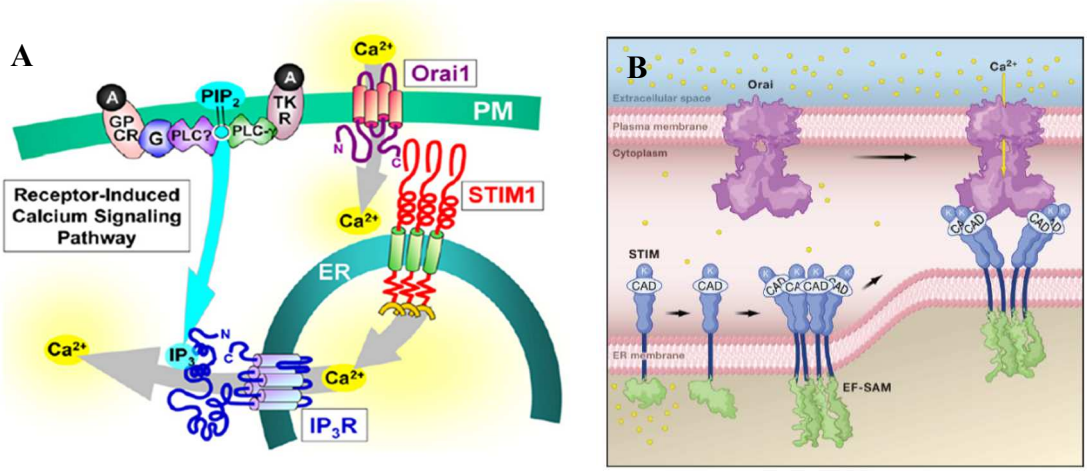

Figure 3: Store operated Ca^{2+} entry signaling. (A) ER lumen Ca^{2+} depletion promotes Ca^{2+} entry through Orai1 (Hewavitharana et al., 2007). STIM1 acts as a Ca^{2+} sensor within the ER. Upon Ca^{2+} depletion mediated by IP_3R or RYRs, STIM1 aggregates in proximity to Orai1 and facilitates CRAC opening for subsequent Ca^{2+} influx, bringing intracellular Ca^{2+} concentrations back to a resting state. **(B) STIM1 aggregation on ER membrane facilitates interaction with Orai1 on plasma membrane (Clapham, 2009).** STIM1 is a multi-domain protein that contains an N-terminal EF-hand pair (Ca^{2+}-binding motif) which is responsible for sensing the lumenal Ca^{2+} concentrations and SAM (sterile alpha motif) domains which are responsible for oligomerization upon Ca^{2+} dissociation (Liou et al., 2005). Orai channels are fully activated by the conserved amino acid fragment 344-448 termed CRAC activation domain (CAD) or STIM1 Orai activating region (SOAR) present on STIM1 (Yuan et al., 2009). In the oligomerized form, STIM1 migrates to the junctional ER directly adjacent to the PM to allow Orai channel opening and Ca^{2+} influx (Miao et al., 2013).

STIM1 (685 amino acid), and its homolog STIM2, are single, transmembrane domain proteins that span the length of the ER membrane and contain a Ca^{2+}-sensing EF-hand domain which faces the ER lumen in its N-terminal region (aa. 23-200) (Figure 4) (Scrimgeour et al., 2014). Upon store depletion, STIM1 forms an oligomer, through protein-protein interactions of the sterile alpha motif (SAM) that is also found on the N-terminus (Manji et al., 2000). Within the SAM domain are contained two N-glycosylation sites which in conjunction with lumenal Ca^{2+} depletion, modulate the rate at which STIM1 accumulates in the junctional ER (or puncta) located within 10-25 nm of the PM (Wu et al., 2006; Kilch et al., 2013). The cytoplasmic or C-terminal region of STIM1 is composed of a

polybasic-lysine rich domain and an essential regulatory domain termed CAD (CRAC activation domain) (Figure 4). Two channel families have been identified as STIM1-regulated SOCs: transient receptor potential (TRP) and Orai channels. Both are differentially regulated based on interactions with the lysine rich domain and CAD of STIM1 (Yuan et al., 2009). The STIM1 lysine-rich domain is essential for TRP channel opening, but inhibits Orai1, whereas the STIM1 CAD binds, but is not sufficient to activate TRP channels, thus providing a regulatory mechanism for SOCE (Yuan et al., 2009). The lysine-rich domain has also been shown to initiate the recruitment of STIM1 to ER-PM junctions to expose a high concentration of CAD sites beneath the PM, which increases the likelihood of binding a diffusing Orai channel (Park et al., 2009).

Orai1 is a 301 amino acid plasma membrane protein, constitutively expressed in most cell types, containing four transmembrane domains with both the N- and C-terminus located within the cytosol (Figure 4). The N-terminus includes a Calmodulin (CaM) binding domain (CMBD), CAD binding domain, and a proline-rich domain. The lysine domain of STIM1 has been shown to downregulate the activity of Orai1 when interacting with the proline-rich N-terminal region by preventing CAD binding (Yuan et al., 2009). The CMBD of Orai1 (residues 68-91) is the conserved binding sequence for CaM, and such an interaction promotes fast Ca^{2+}-dependent inactivation (CDI) of the Orai1 channel (Mullins et al., 2009). The cytosolic intracellular loop, also contained within the cytosol, is highly conserved within the Orai family (Orai1, 2, and 3) and between species, where it has been shown to act as a channel inactivation gate (Frischauf et al., 2009; Srikanth et al., 2009). The C-terminus of Orai1 contains the preferential CAD binding site (residues 268-291), where upon interacting

with STIM1, the Orai1 channels fully assembles and undergoes a conformational change to promote channel opening and Ca^{2+} influx (Yuan et al., 2009; Park et al., 2009).

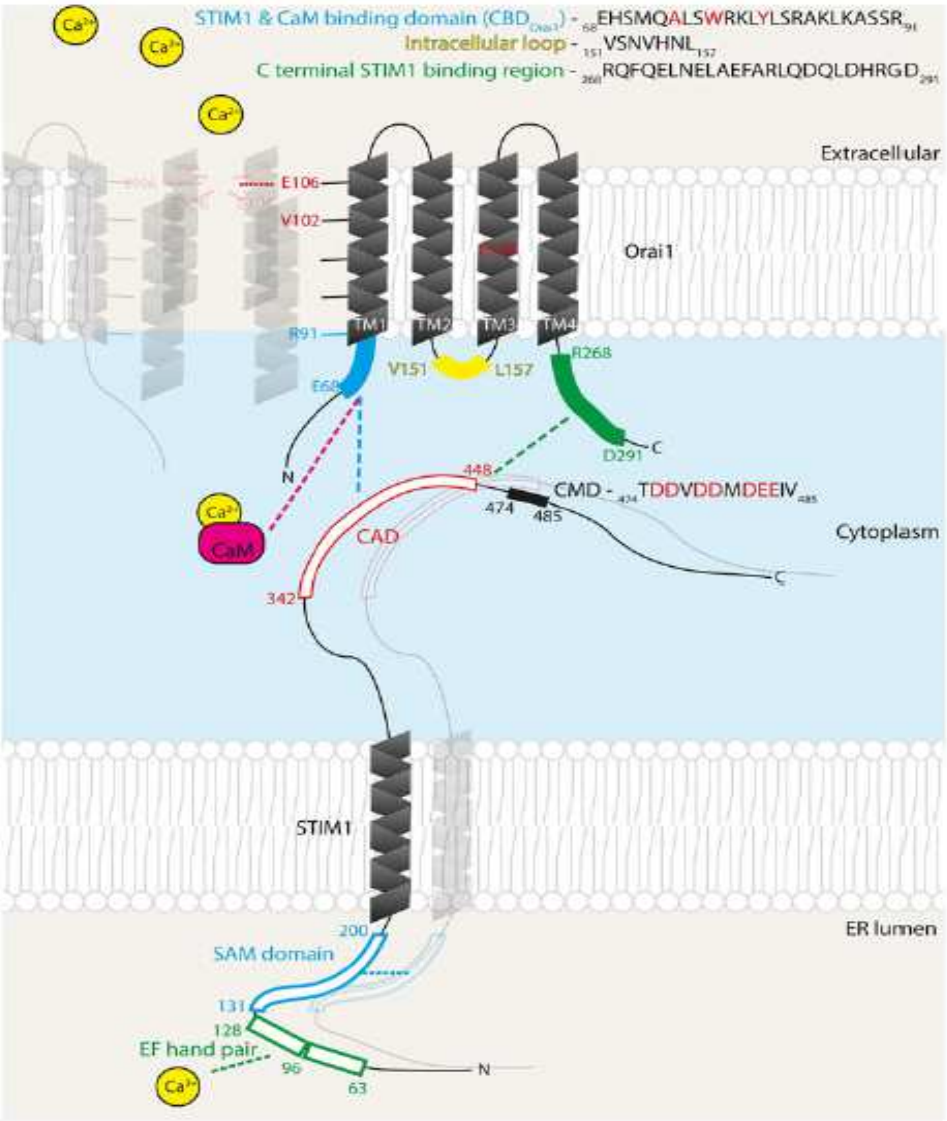

Figure 4: Diagram of the STIM1/Orai1 complex and key domains (Scrimgeour et al., 2014). The key domains of STIM1 are the Ca^{2+}-binding EF-hand motifs (green boxes), the SAM domain required for STIM1 oligomerization upon Ca^{2+} depletion (cyan box), CRAC activating domain (CAD) which binds to both the C- and N-terminal of Orai1 (red box), and the CRAC modulatory domain (CMD) (black box). The key domains of Orai1 are the CaM binding domain/CAD binding domain (cyan), the intracellular loop (yellow), and the C-terminal STIM1 CAD binding region (green). Orai1 is depicted on the PM, where transmembrane domain 1 lines the channel pore with the selectivity filter formed by a hexameric ring of E106 residues.

The first transmembrane domain of each Orai1 subunit is believed to be responsible for CRAC channel formation, where the E106 residue forms the pore selectivity center, similar to what has been reported for L-type Ca^{2+} channels (Tang et al., 1993; Yang et al., 1993). The selectivity of E106 was confirmed by a point mutation to glutamine (E106Q) or alanine (E106A), showing a dominant, negative effect in which CRAC current was suppressed (Prakriya et al., 2006; Vig et al., 2006a). Interestingly, an Orai1 channel E106D mutation (conservative mutation of glutamate to aspartate) retains channel activation when coexpressed with STIM1, but has altered selective permeation (Yeromin et al., 2006) and Ca^{2+}-dependent inactivation properties (Scrimgeour et al., 2012).

While the activation mechanism of the Orai1 channel has been well documented, the subunit stoichiometry of the CRAC channel remains speculative. It was initially suggested that the Orai1 pore functions as tetramer (Ji et al., 2008), but recent data from the crystal structure of the *Drosophilia melanogaster* homolog of Orai1suggests that the pore is surrounded by six transmembrane 1 domains of Orai1 to form a hexameric channel (Hou et al., 2012). Studies have also indicated that varying the expression levels of STIM1 and Orai1 alter Ca^{2+}-dependent inactivation rates and change preferential selectivity to divalent cations other than Ca^{2+} (Scrimgeour et al., 2009). The 1:2 (Orai1:STIM1) stoichiometry has been shown to produce the maximal I_{CRAC} (Ca^{2+} influx current) and promote fast channel inactivation, whereas a 1:1 stoichiometry exhibits smaller whole cell currents and Ca^{2+}-dependent reactivation of I_{CRAC} (Li et al. 2011; Hoover and Lewis, 2011).

In light of the *Drosophila* Orai crystal structure, it has been suggested that STIM1 binds at three different sites per channel as CAD interacts with both the N- and C-terminals of Orai1 (Hou et al., 2012). However, this contradicts the idea of 2 STIM1 binding to 1

Orai1 for maximal I_{CRAC} and that STIM1-CAD forms a tetramer in solution (Park et al., 2009). Hypothetically, if STIM1 were to exist in an extended conformation, this may permit twelve binding sites, in which the differences in binding affinity between the C- and N-terminal Orai1 may control reactivation and inactivation of the channel. For example, when lumenal Ca^{2+} concentrations are relatively full and STIM1 is primarily concentrated away from the PM, CAD may only interact with the C-terminus, which would favor Ca^{2+}-dependent reactivation (Scrimgeour et al., 2014). However, when STIM1 saturates the junctional ER upon decrease in lumenal Ca^{2+} concentrations, CAD may interact with both the C- and N-terminus to eventually promote channel inactivation (Scrimgeour et al., 2014). As one can see, channel inactivation is a complex process, which is affected by channel subunit stoichiometry, the cytoplasmic domains of both STIM1 and Oria1, the selectivity center within the Orai1 pore, and more recent evidence showing protein modulation.

Ca^{2+}-dependent inactivation (CDI) is a critical regulatory mechanism of CRAC channels in that it ensures efficacious intracellular Ca^{2+} signaling by regulating the cytosolic and extracellular Ca^{2+} concentrations to maintain a steep gradient. Two protein modulators have been shown to promote CDI of CRAC channels: 1) the Ca^{2+} sensor protein Calmodulin (CaM) which promotes fast CDI (order of milliseconds) and 2) the ER resident membrane protein SOCE-associated regulatory factor (SARAF) which initiates a slower CDI. SARAF is highly conserved and has exceptionally high transcript levels in mammalian neuronal and immune tissues (Su et al., 2004). It has been shown that in response to elevated cytosolic Ca^{2+} concentrations, SARAF promotes a slow inactivation process by both inhibiting spontaneous activation of STIM1 and enhancing STIM1 deoligomerization upon store refilling (Palty et al., 2012). The STIM1 C-terminal inhibitory domain (CTID) (residues

448-530) physically dictates the interaction of STIM1 CAD with SARAF, which prevents Orai1 activation (Jha et al, 2013). However, at this stage, it is left to speculation on how SARAF mediates its functional activities in a Ca^{2+}-dependent manner. It has been proposed that an EF-hand containing cytosolic protein termed CRAC regulator 2A (CRACR2A) may form a complex with SARAF upon local elevation of Ca^{2+} near the PM as it dissociates from its role in stabilizing the STIM1/Orai1 complex (Palty et al., 2012; Srikanth et al., 2010). While the mechanistic details for how SARAF promotes slow CDI in a Ca^{2+} dependent manner remain largely to be determined, those pertaining to CaM's fast CDI have been better characterized based on Ca^{2+} dependency.

In 2009, *Mullins et al.* determined the main regulatory mechanism for fast CDI, identifying a membrane proximal N-terminal domain of Orai1 (residues 68-91) (Figure 4) that binds CaM in a Ca^{2+}-dependent manner. As CaM interacts through primarily hydrophobic surfaces contained on target amphipathic helices (O'Neil and DeGrado, 1990), point mutations made on residues on Orai-CMBD believed to be involved in the binding interface (A73E, W76E, Y80E) depicted disruption of CaM binding and inhibition of inactivation of I_{CRAC}, providing strong evidence that CaM binding to the N-terminus of Orai1 is required for CDI (Mullins et al., 2009). In contrast, Orai-CMBD mutations of Y80A and Y80S not only retained CaM binding, but also enhanced CDI (Mullins et al., 2009). Given that both the E106D in the Orai1 channel pore selectivity filter and the Y80A/Y80S mutation in the N-terminal of Orai1 promote fast acceleration of CDI, it may be that the E106D mutation allosterically modulates the CaM binding domain of Orai1, or the pore and/or CMBD mutants cause a similar change in the affinity of Ca^{2+} binding within the pore to regulate CDI (Scrimgeour et al., 2014). The interplay between CaM binding and pore

selectivity has been suggested as an inactivation mechanism for Ca_v 1.2 channels, where CaM binding to the cytoplasmic side of the channel increases the affinity of the selectivity filter for Ca^{2+} ions, causing excess Ca^{2+} ions to become trapped within the pore to prevent further influx (Babich et al., 2007). Alternatively, it has been proposed that CaM binding to Orai1 dissociates STIM1 CAD from its N-terminal binding site, as these binding sites overlap (Park et al., 2009). Whether or not the pore mutation prevents CaM binding via an allosteric effect has yet to be determined, but the best working hypothesis for CDI is that upon Ca^{2+} influx, CaM senses high intercellular Ca^{2+} concentrations and binds to the N-terminal of Orai1. However, such binding does not displace STIM1 CAD, but instead promotes the interaction with the CRAC modulatory domain (CMD) (residues 474-485 on STIM1), which then inactivates Orai1, bringing the channel into a nonconducting state (Lee et al., 2009; Mullins et al., 2009), which is independent of the E106D channel mutant.

In addition to promoting I_{CRAC} inactivation, CaM promotes inactivation of voltage gated Ca^{2+} channels (Levitan, 1999; Saimi and Kung, 2002) and slow inactivation/reactivation (on the order of tens of seconds) for L-type Ca^{2+} channels, through direct interaction with the IQ (isoleucine-glutamine) motif (Zuehlke et al., 1999). CaM has also been shown to inactivate TRPC1 channels, in which expression of a Ca^{2+} insensitive CaM mutant resulted in both a decrease in CDI and an increase in current influx (Singh et al., 2002). While CaM's role in Ca^{2+} channel inactivation has been well documented, the mechanistic details of the inactivation processes still remain largely speculative.

1.3 Physiological Significance of SOCE

Ca^{2+} signaling remains a forefront cellular process as it mediates nerve and muscle relaxation, regulation of blood pressure, cognition, sensory transduction, and cell proliferation, to name a few. Altered Ca^{2+} signaling in relation to SOCE has been shown to cause numerous pathological phenotypes. In patients lacking the functional CRAC channel, it has been shown that lymphocytic cells were unable to mount suitable immune responses as a consequence of impaired SOCE and cytokine production (Feske et al., 2005; Feske et al., 2006; Vig and Kinet, 2009). STIM1 functionally deficient patients also have presented muscular hypotonia and chronic pulmonary diseases as a result of defective respiratory muscle functions (Picard et al., 2009). Orai1 was first identified for its functionality in CRAC channels by a prevalent point mutation (R91W) in patients with severe combined immunodeficiency (SCID) syndrome (Feske et al., 2006). The R91W mutation, present in the first TM domain of Orai1, disrupts CRAC channel formation, but does not disrupt the Orai1/STIM1 interaction or alter Orai1 expression on the PM (Feske et al., 2006; Navarro-Borelly et al., 2008). This missense mutation likely gates and/or interferes with CRAC channel opening by reducing the mobility of the first TM domain of Orai1 within the lipid bilayer, as only R91 substitution with hydrophobic, but not neutral or charged amino acid residues curtails I_{CRAC} (Derler et al., 2009; Zhang et al., 2011). Such a loss of function mutation induces inadequacies of Ca^{2+} influx, downregulating the NFAT pathway, resulting in diminished T-cell activation and the inability to mount an immune response (Macian, 2005; Feske et al., 1996). Given that the treatments for SCID at best consist of hematopoietic stem cell transplantation, further exploration of the mechanistic roles of CRAC channel reactivation/inactivation is an expanding and promising avenue for drug development.

1.4 EF-Hand Superfamily and Its Members: Calmodulin and Troponin C

Ca^{2+} binding proteins (CaBPs) are grouped according to the nature of their associated binding motifs. The predominate motifs that encompass most Ca^{2+} binding proteins are the all α-helical EF-hand motifs (EFs), the all β-sheet C2 domains, and the Greek key motif βγ-Crystallins. EF-hands are typically composed of two α-helices bridged by a loop to form a helix-loop-helix motif (Figure 5). The looped structure is flexible and provides the highly conserved chelation ligands, such as negatively charged glutamate and aspartate residues for Ca^{2+} binding. The typical coordination of the Ca^{2+} ion consists of seven ligands in a pentagonal bipyramidal geometry, with one of the seven ligands involved in the coordination being a water molecule (Gifford et al., 2007). Two types of notation for the chelating residues are typically employed, either being annotated by their linear position within the loop or by their tertiary geometry on the axes of the pentagonal bypyramid: 1(+X), 3(+Y), 5(+Z), 7(-Y), 9(-X), 12(-Z). The residues 1, 3, 5, 7, 9, and 12 all participate in the chelation of Ca^{2+} and are most commonly Asp, Asp, Asp, Thr, Asp, and Glu, respectively (Gifford et al., 2007; Lewit-Bentley and Réty, 2000).

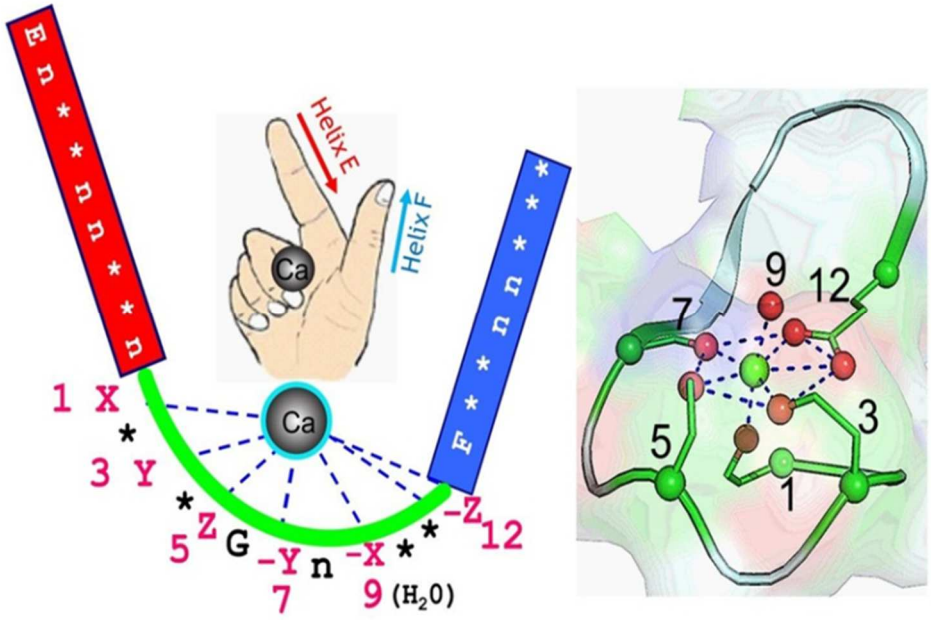

Figure 5: EF-hand motif structure and ligand coordination for Ca^{2+} chelation (Gifford et al., 2007). The structural arrangement of an EF-hand motif depicts the "E" α-helix as the finger, the Ca^{2+} chelation loop as the palm, and the "F" α-helix as the thumb, using the hand analogy. Residue 1 (typically Asp) within the chelation loop dictates the stereochemical arrangement. Typically, the smallest residue glycine is present in the sixth position, which makes the 90° turn to allow the remaining Ca^{2+} chelating ligands to be in coordinating positions. The eighth residue is a highly conserved hydrophobic residue (typically Ile) which enables a short anti-parallel β-sheet to form. The formation of an anti-parallel β-sheet is a result of the main chain amine and carbonyl groups facing away from the Ca^{2+}-binding site towards the loop of the EF-hand. The 12th position lies within the helices instead of the loop and is bidentate, providing two coordination ligands. This residue is almost exclusively Glu.

In comparing EF-hand motifs with C2-domains and βγ-Crystallins, EF-hands exhibit moderate to very high Ca^{2+} affinities with K_d values in the nanomolar range, whereas C2 and βγ-Crystallins domains exhibit affinities on the μM range (Gifford et al., 2007). Most major domain categories show little or no binding towards Mg^{2+}, exhibiting high selectivity for Ca^{2+} (Nalefski and Falke, 2002). Mg^{2+} has been documented to bind to Ca^{2+}-specific/regulatory EF-hands, albeit with weak affinity (Gifford et al., 2007) and minimal conformational change from the apo-CaBP form (Wei et al., 2010). Those CaBPs that contain EF-hands typically undergo large conformational changes upon Ca^{2+} binding

(Lewit-Bentley and Réty, 2000), whereas C2 and βγ-Crystallins generally exhibit no significant conformational changes when bound to Ca^{2+}, suggesting the apo forms are not very conformationally flexible (Wenk and Jaenicke, 1999). Interestingly, while βγ domains do not undergo major structural change when binding Ca^{2+}, they assume a reduced hydronamic size (Suman et al., 2013; Srivastava et al., 2010) as indicated by dynamic light scattering and gel filtration chromatography, and become thermodynamically stabilized, similar to other EF-hand containing CaBPs (Suman et al., 2013, Yamnuik et al., 2009). Lastly, both C2 and βγ domains are discontinuous in their Ca^{2+}-binding sites and are formed by distant regions within the primary sequence (Sutton et al., 1995), whereas EF-hand domains always bind Ca^{2+} within the continuity of the looped linking region (Yang et al., 2002; Pidcock and Moore, 2001). The remarkable variability in both structure and Ca^{2+} coordination amongst the major domains is essential for CaBPs to mediate the diverse array of Ca^{2+}-dependent sensing and signal transduction.

Calmodulin (CaM) is a 17 kDa, (148 amino acids) acidic protein which plays important roles in Ca^{2+}-dependent signal transduction in eukaryotes as it is able to act as a Ca^{2+} sensory mediator for many enzymatic reactions, being able to bind to some 300 different amino acid sequences (Kursula, 2014a). There are a number of CaM target molecules that have been identified, including, to name a few, protein kinase, protein phosphatase, nitric oxide synthase, tRNA, Ca^{2+} pump, and proteins involved in motility and T-cell activation (Clore et al., 1993). CaM is a Ca^{2+} sensor protein in non-muscle cells, which binds four Ca^{2+} ions through its self-contained four Ca^{2+} binding EF-hands. The structure of CaM is arranged into two separated globular lobes, each containing a tandem pair of EF-hands, with a flexible tether in between. Ca^{2+}-free CaM adopts a so-called closed structure, in which the two lobes

come in close proximity of each other by burying most of their hydrophobic residues. Ca^{2+} binding to CaM triggers a major conformational change to form an extended dumbbell-shaped structure, linked by a solvent-exposed, rigid helical structure in x-ray crystallography (Babu et al., 1985; Babu et al., 1988; Kretsinger et al., 1986) but an un-structural linker in NMR (Ikura et al., 1992a), suggesting both structures may coexist in solution to facilitate target complexation.

The mechanism for CaM to recognize its target molecules is primarily through strong hydrophobic interactions, in which Ca^{2+} binding to CaM exposes its hydrophobic patch, allowing CaM to interact with the CaM-binding domain (CMBD) of a target molecule followed by enzyme activation. A CMBD typically is comprised of 15-35 amphipathic amino acids (interspersion of basic and hydrophobic residues) with high propensity for helix formation, which shows an un-structural conformation in solution but forms an α helix when complexed with CaM. The CMBD sequences are considerably divergent. There are several structures of CaM/CMBD complexes that have been determined, including those that fall under the category of the well-documented canonical model (Figure 6). In this model, each lobe of CaM interacts with the different ends of a CMBD peptide in a sequential manner; first binding to the C-terminal lobe followed by the N-terminal lobe (Bayley et al., 1996; Sun and Squier, 2000). To achieve this, CaM's helix linker is disrupted and extended, forcing the structure to "collapse" to grip the peptide (Meador et al., 1992). Despite the overall structural change, NMR reveals that there is no significant conformational change within each lobe between the uncomplexed and complexed states (Ikura et al., 1992b). Classic examples of this canonical binding include CaM/M13 and CaM/CaMKII.

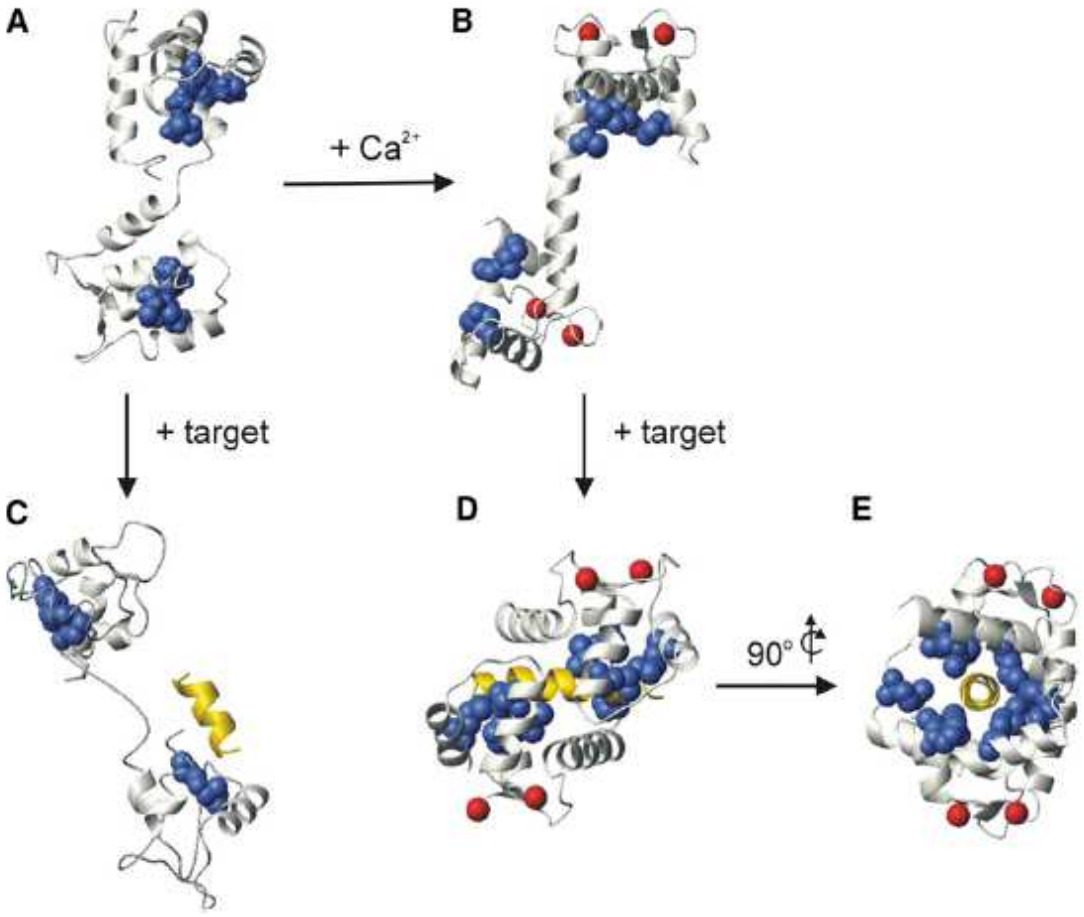

Figure 6: Apo- and Ca^{2+}-bound CaM structures and target interactions (Yamnuik et al., 2009). CaM consists of two globular domains (the N-terminus containing the 1st and 2nd EF-hands and the C-terminus containing the 3rd and 4th EF-hands) connected by a central helix linker, which typically bends to allow hydrophobic regions to interact with target proteins (Figure 2B->D). In the absence of target proteins, the central linker is typically flexible in solution and the N and C terminal lobes of CaM do not interact with one another. When bound to a target in the Ca^{2+} form, the N and C lobes wrap around the CMDBs (typically α-helical in nature) shown here in a collapsed 1:1 binding mode. **(A) Apo-CaM (PDB:1DMO). (B) Ca^{2+}-CaM (PDB:1CLL). (C) Apo-CaM in complex with the SK channel CaM binding domain peptide (PDB:1QX7). (D) Ca^{2+}-CaM complexed with the smMLCK peptide (PDB:1CDL). (E) 90º y-axis rotation of complex D.** Here hydrophobic Met residues (blue) are represented as spaced-filled globular structures, Ca^{2+} ions as (red) spheres and bound target peptides as (yellow) ribbons.

Alternatively, other CaM/CMBD complexes have been observed in a non-canonical manner, in which CaM binds target CMBDs with a 1:1, 1:2 or 2:2 mode (for review, see Kursula, 2014a). Despite that the current understanding for recognition allows one to predict

the possible CMBD sequences in target enzymes or proteins assisted with the CaM target database (Yap et al., 2000), the mode of CaM/CMBD recognition still remains to be elucidated only by experimental approaches, indicating that the hydrodynamic properties of CaM and its associated physiochemical properties are not well understood. Additionally, the disparity in binding conformations is consistent with the lack of sequence homology among CMDBs, making it challenging to use existing structural information to accurately predict the interaction of CaM and target proteins (Liu et al., 2012). Therefore, there is still a need to understand the structural basis of the interaction between CaM and its target proteins. An advance in this knowledge will eventually lead to a better understanding of CaM's diverse regulatory functions.

In the past, chimeras of CaM and Troponin C (TnC) have been utilized to help elucidate the binding mechanism to their target proteins. TnC is another member of the EF-hand superfamily, and has direct roles in promoting skeletal muscle contraction. CaM and TnC share only 50-70% homology at the amino acid level but they possess striking structural similarities, as shown in the crystal structures of CaM and skeletal TnC (sTnC). Both CaM and TnC contain four EF-hands but have an opposite effect in the activation of target enzymes. For example, TnC can neither bind to nor activate nNOS (Su et al., 1995) and has a very low affinity for Ca^{2+}-ATPase (CA) (Fidalgo Da Silva et al., 2006). Given the structure similarities and functional differences of CaM and TnC, chimera proteins, in which the domains containing EF-hands of CaM are exchanged with the corresponding EF-hands of TnC, and vice versa, allow for the investigation of the functionality of each specific protein. For example, chimeras of CaM, where each includes one of four domains (either the 1st EF-hand (EF1), EF2, EF3 or EF4) from TnC have been constructed, including CaM(1TnC)

(domain 1 of TnC and domains 2, 3, and 4 of CaM), CaM(2TnC), CaM(3TnC), and CaM(4TnC), as well as other multiple-domain exchange chimeras. The sequences of the constructs from human CaM (hCaM) and cardiac TnC (cTnC) are summarized in Figure 7. Notable sequence differences among the chimeras include: 1) CaM(1TnC) contains additional N-terminal residues and its EF1 is non-canonical in that it does not bind Ca^{2+}, and 2) CaM(2TnC) has three extra residues in its central helix. Besides the sequence difference, TnC also has different Ca^{2+} binding properties. TnC's EF4 has a one order higher Ca^{2+} affinity than that of CaM, and its second helix of EF2 (i.e. helix D) is oriented differently compared to that of CaM (George et al., 1996). These chimeras have been used in the studies of CaM/NOS (Su et al., 1995; Gachhui et al., 1998; Newman et al., 2004) and CaM/Ca^{2+}-ATPase interactions (Fidalgo Da Silva et al., 2006). It is assumed that these chimeras adopt a similar structure as CaM, and therefore interact with CMBDs similarly. Thus, the change of functionality, such as enzyme activation, can be explained mainly by the lack of the association of specific elements in the chimeras (due to the subtle sequence differences and/or side chain packing) and specific domains in the target macromolecules. In some cases, the failure of stimulating enzymatic activation is explained by the lack of complex formation due to the exchanged domains (Strynadka and James, 1990). However, whether or not such exchanged EF-hands have an impact on chimera protein structure, including hydrophobic exposure, as well as CMBD interactions, has yet to be addressed.

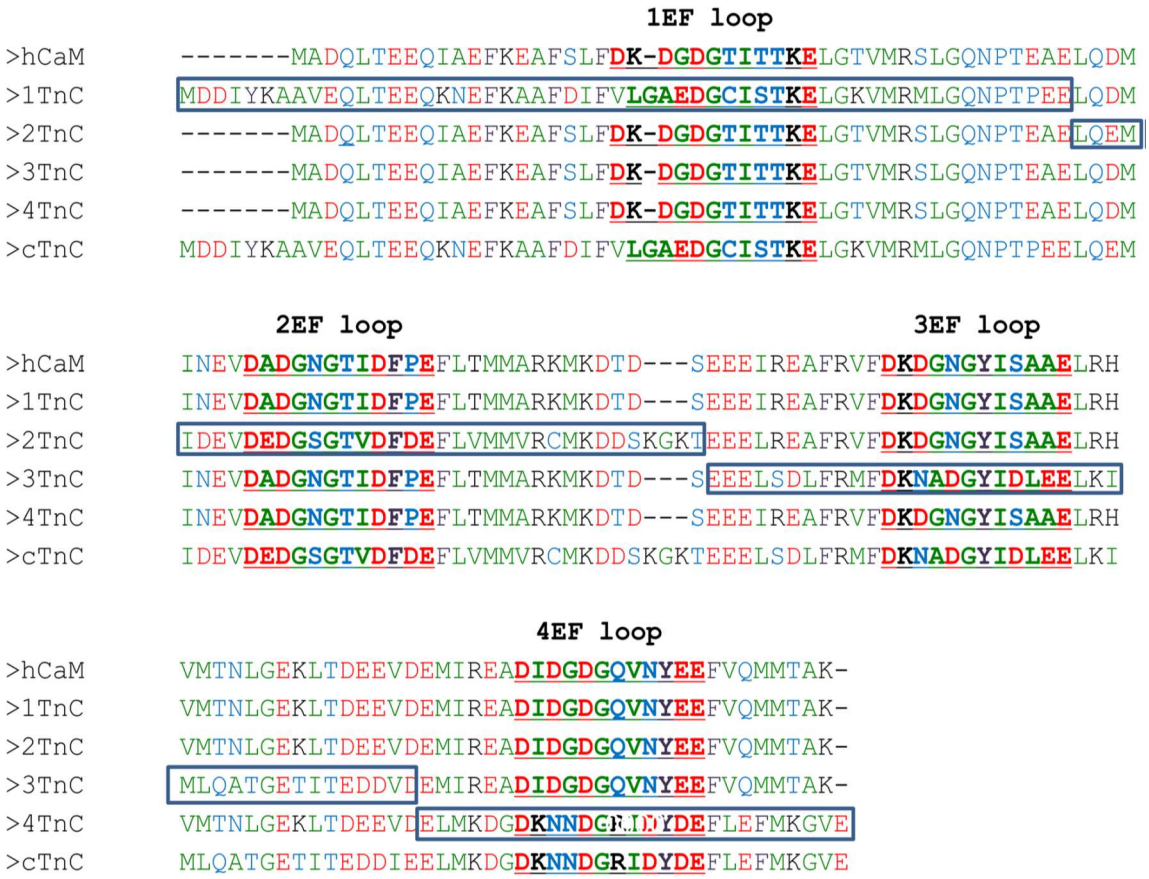

Figure 7: Sequence alignment of hCaM, cTnC and chimeras. Sequence alignment was performed with ClustalW. Residues are colored coded in terms of amino acid properties where green are hydrophobic, blue are polar/uncharged, black are positively charged, red are negatively charged and brown are aromatic. The four, 12-residue EF-hand Ca^{2+} binding loops are depicted in bold and underlined. The corresponding sequences from cTnC added to create the individual chimeras are outlined with boxes.

1.5 Statement of Purpose

As Ca^{2+}-induced hydrophobicity of CaM is generally believed to be important for its ability to recognize CMBDs, here, through spectroscopy and calorimetry, we first utilized the ANS fluorescent probe to assess the extent of hydrophobicity and structural change of CaM and the four chimera proteins upon Ca^{2+} binding. We then studied the interaction of CaM with a peptide corresponding to the CMBD of Orai1 (Orai-CMBD) and further extended the

studies to the chimera proteins themselves. We hypothesized that the hydrophobicity change in chimeras may have an impact on their interaction with Orai. Additionally, given the fundamental differences between CaM and TnC, we anticipate that these chimeras will serve as an informative probe to better understand the interaction between CaM and Orai-CMBD and therefore, could be used to extend to studies using the full length of the Orai channel protein as well as to other CaM/CMBD systems. While the mechanistic details of how CaM promotes CDI of CRAC channels remain elusive, by using isothermal titration calorimetry and stopped-flow kinetics, we hope to provide the physical basis of the molecular inactivation. Additionally, by using circular dichroism and fluorescence quenching, we hope to elucidate the chemical environment of Orai-CMBD CaM binding. During our characterization, an excellent work published by *Liu et al*. (2012) showed that CaM binds to Orai's CMBD in an unusual 1:2 open conformation mode. Thus, we rationalized our experimental data to accommodate their model.

CHAPTER 2

EXPERIMENTAL

2.1 General

All chemicals were purchased from Sigma-Aldrich (St. Louis MO) and Fisher Scientific (Pittsburgh PA), and used without further purification. The peptide sequence corresponding to 68-91 residues of Orai1, $_{NH2}$-EHSMQALSWRKLYLSRAKLKASSR-$_{COOH}$, was purchased from NEO BioLab (Cambridge MA). Buffers needed to be made Ca^{2+}-free were treated with Chelex-100 (Bio-Rad Laboratories, Hercules CA) prior to use. All characterization measurements were performed at least three times using three different protein batches, and the results were reproducible.

2.2 Recombinant Protein Expression/Purification

Chimera proteins, CaM(1TnC), CaM(2TnC), CaM(3TnC), and CaM(4TnC) were obtained as a generous gift from Dr. George (Duke University School of Medicine). The gene inserts for CaM(1TnC), CaM(2TnC) and CaM(4TnC) were cloned to an expression plasmid operated by the bacteriophage λ P_L promoter. For a detailed description of the plasmid construction and cloning, see *George et al.* (1993). For an overview of λ P_L promoter vector construction and uses in protein expression, reference *Cheng and Patterson* (1992). CaM and CaM(3TnC) were subcloned to a pLW-His_6 vector under control of the Lac promoter.

2.2.1 Transformation of plasmid DNA to obtain glycerol cell stocks

BL21 (DE3) Competent *E. coli* cells from New England BioLabs, Inc. (Ipswich MA) were thawed on ice for 5 min before approximately 50 ng of plasmid DNA containing the gene inserts for CaM and the chimeras was added separately to the cell mixture. Cells were then placed on ice for 30 min, followed by heat shock at 42°C for exactly 10 sec. The transformed cells were then incubated on ice for an additional five min before adding 950 µL SOC medium to the cell mixture. The cells were then shaken at 250 rpm for 60 min at 37°C (New Brunswick Scientific I26 incubator shaker, Edison NJ). Meanwhile, a selective agar plate was prepared, containing 100 µg/mL of ampicillin (Amp) (Gold Biotechnology, St. Louis MO). This was accomplished by heating a 2% agar solution in autoclaved Luria Broth (LB) medium until the agar powder was completely melted. Once the mixture was cooled to 50-60°C, 10 mL of LB agar solution was poured into a sterile petri dish containing the specified Amp concentration and was left to solidify. 25-50 µL of the cells were then spread evenly over the selection plate and incubated inverted overnight at 37°C in an incubator (Thermo Scientific Heratherm™ Incubator, Waltham MA) to promote vertical growth of the cell colonies. The following morning, a single, isolated colony was added to 5 mL LB medium with 100 µg/mL Amp and was shaken at 37°C, 220 rpm until the mixture became cloudy. 500 µL of the culture cells were then used to make a 25% glycerol stock suspension that was stored at -80°C until further use.

2.2.2 Recombinant protein expression

2.2.2.1 CaM and CaM(3TnC)

First, an Amp selection plate was made as in *2.2.1*. Then approximately 10 µL glycerol stock cell culture containing pLW-His_6-CaM or pLW-His_6-CaM(3TnC) was added into 5 mL LB. 100 µL of the resulting mixture was spread evenly over the solidified agar plates. The plates were inverted and incubated overnight at 37ºC. The following day, a single isolated colony was scraped from the plate and inoculated into 10 mL of LB medium containing 100 µg/mL Amp. The mixture was shaken at 220 rpm, 37ºC until becoming cloudy. The saturated culture was then up-scaled with 1-4 L of fresh LB medium containing 25 µg/mL of Amp in 2 L Erlenmeyer flasks, each containing less than 500 mL of culture media. The culture was further shaken at 37ºC until an optical density (OD) of 0.4-0.6 was reached. The optical density was determined at 600 nm (OD_{600}) with an Ultrospec 10 cell density meter **(**Amersham Biosciences, Piscataway NJ**)**, using LB medium as a reference. Once the desired OD_{600} was attained, the culture was induced with 0.5 mM Isopropyl-β-D-1-thiogalactopyronoside (IPTG) (Gold Biotechnology, St. Louis MO) and continuously expressed for 3-4 hours at 250 rpm and 37ºC. The cells were harvested at 4ºC via floor centrifugation for 10 minutes at 6,000 rpm (Beckman Sorvall® RC 5B Plus, Pasadena CA). The resulting cell pellet was homogenized in 6X the pellet weight of ice cold lysis buffer (50 mM Tris, pH 7.5, 0.5 M NaCl). The mixture was flash frozen in liquid nitrogen and stored at -80ºC for eventual protein extraction/purification.

2.2.2.2 CaM(1TnC), CaM(2TnC), and CaM(4TnC)

Purification methods were adapted from *George et al.* (1990). The agar plate was made in a similar manner as in *2.2.1*. Then approximately 10 μL glycerol stock cell culture of cells transformed with the plasmids containing the cDNA of CaM(1TnC), CaM(2TnC), and CaM(4TnC) was added into 5 mL LB. 100 μL of the resulting mixture was spread evenly over the solidified agar plates. Plates were incubated for two days at 30ºC (Barnstead Lab-Line L-C Incubator, Waltham MA). A single, isolated colony was scraped from the plate and inoculated into 10 mL of LB medium containing 100 μg/mL Amp. The mixture was shaken at 220 rpm, 30ºC for approximately 10 hours or until becoming cloudy. The saturated culture was then up-scaled to 2 L of LB medium containing 50 μg/mL Amp in 2 L Erlenmeyer flasks, each containing 500 mL of culture media The culture was shaken at room temperature until OD_{600} reached 1.0. The protein expression was induced by adding another 2 L of LB medium heated at 65.5ºC with 50 μg/mL Amp and continuously shaken for 4-6 hours at 250 rpm and 42ºC. The cell pellets were obtained as in *2.2.2.1* and the cell homogenate was stored at -80ºC for eventual protein extraction/purification.

2.2.3 Cell lysis and protein extraction

The cell homogenates from *2.2.2.1* and *2.2.2.2* were thawed in an armor bath (Fisher Scientific Isotemp 105, Waltham MA). Once thawed, 15 mL fractions of the cell culture were sonicated (Fisher Scientific Sonic Dismembrator Model 500, Waltham MA) for 4 min with the pulse on for 30 sec and then off for 30 sec, to minimize protein denaturation due to heat. The lysate was centrifuged at 12,000 rpm and 4ºC for 15 min and the resulting pellets were discarded.

2.2.4 Recombinant protein purification

2.2.4.1 CaM, CaM(1TnC), CaM(2TnC), and CaM(4TnC)

Purification of CaM and all other chimeras excluding CaM(3TnC) was performed at 4ºC using hydrophobic interaction chromatography (HIC). The supernatant obtained in section *2.2.3* was incubated with 3 mM Ca^{2+} for 5 min and then centrifuged for 60 min at 12,000 rpm and 4ºC. The supernatant was then loaded onto a 2.5 x 10 cm column containing approximately 15 mL of phenyl sepharose resin (Amersham Biosciences, Piscataway NJ) that was previously equilibrated with approximately 50 mL of 50 mM Tris, pH 7.5, 5 mM Ca^{2+}. The column was then washed successively with 0.5-1 L of 50 mM Tris, pH 7.5, 0.5 mM Ca^{2+}; 0.1-0.2 L of 50 mM Tris, pH 7.5, 0.5 mM Ca^{2+},0.5 M NaCl; and 0.1 L of 50 mM Tris, pH 7.5, 0.5 mM Ca^{2+}. The desired protein was eluted using 50 mL of 50 mM Tris, pH 7.5, 5 mM EDTA. Using an Amicon Ultra centrifugal filter device with a 3 kDa molecular weight cut off (MWCO), the elutant was centrifuged at 3,500 rpm and 4ºC (Thermo Scientific Sorvall® Legend XTR, Waltham MA) and concentrated to approximately 1 mL. Using HIC, CaM yielded approximately 15-20 mg per liter of bacterial culture, whereas CaM(1TnC), CaM(2TnC), and CaM(4TnC) yielded approximately 5 mg per liter.

2.2.4.2 CaM(3TnC)

As we observed that CaM(3TnC) was unable to be retained on the phenyl sepharose resin, it was purified through a Ni-NTA column that interacts with the additional His_6 tag in the N-terminal of the protein. The supernatant obtained in section *2.2.3* was loaded onto a 2 cm column containing approximately 15 mL of Probond Ni-NTA resin (Invitrogen, Grand Island NY) set-up for FPLC purification (GE AKTAprime plus, Pittsburgh PA). The column

was equilibrated and washed with 50 mM Tris, pH 7.5, 0.5 M NaCl. The protein was eluted in 1 mL fractions over a gradient using 50 mM Tris, pH 7.5, 40 mM imidazole. The fractions containing the purified protein were combined and concentrated as in *2.2.4.1*, yielding approximately 10 mg per liter of bacterial culture. Note that CaM can also be purified using Ni-NTA chromatography as the vector also contains the N-terminal His_6 tag. However, we observed better purity and/or yield when using HIC.

2.3 Preparation of Ca^{2+}-Free Proteins

To render the proteins Ca^{2+}-free, the concentrated samples were incubated with 20 mM EDTA, and either dialysed against 1 L of 50 mM Tris, pH 7.5,1 mM EDTA overnight at 4ºC or immediately subjected to three buffer exchanges with Chelex-treated buffer (50 mM Tris, pH 7.5, 1 μM EDTA) in an Amicon Ultra centrifugal filter device (3 kDa MWCO) and concentrated to approximately 0.5 mL. Proteins then underwent three-four additional buffer exchanges in the desired buffers for experimental characterization.

2.4 Determination of Protein Concentration and Purity

Protein concentration was determined with a Bradford assay using bovine serum albumin (BSA) as a standard as reported previously (Liu et al., 2012). The absorbance change of Coomassie Brilliant Blue G-250 Protein Assay Reagent (Thermo Scientific, Waltham MA) was monitored at 595 nm using a 96 well plate reader (μQuant Bio-Tek Instruments Inc., Winooski VT). In addition, the concentration of CaM was also determined by UV-Vis (Shimadzu UV-1800, Kyoto Japan) at 278 nm with a molar extinction coefficient of 1550 $M^{-1}cm^{-1}$ (Shixing and Haug, 1988). The protein purity was checked via 15% SDS-

PAGE. Its purity was estimated to be > 95% based on density profiles measured using UN-SCAN-IT software (Silk Scientific, Inc., Utah).

2.5 Dansyl Chloride Labeling

Dansylation of CaM and chimeras was adapted elsewhere (Kincaid et al., 1982). 15-20 mg of CaM and chimeras were first buffered exchanged in 0.1 M sodium bicarbonate, pH 9.0, three times. 50 µL of 0.75 M dansyl chloride (Acros Organics) in dimethyl formamide (DMF) was added into the resultant protein solution in the presence of 2 mM Ca^{2+}, with a final volume of 10 mL. The solution was wrapped in aluminum foil and rotated overnight at 4ºC. The following morning, the solution was centrifuged at 13,000 rpm, 4ºC (Fisher Scientific accuSpin Micro 17R, Waltham MA) to pellet any excess dye. The supernatant was then subjected to three buffer exchanges with Chelex-treated 50 mM Tris, pH 7.5, 1 µM EDTA and concentrated to approximately 1 mL. The concentration of the label was determined via UV-Vis (Shimadzu UV-1800, Kyoto Japan) using a molar extinction coefficient of 3400 M^{-1} cm^{-1} at 334 nm (Kincaid et al., 1982).

2.6 Isothermal Titration Calorimetry

The ITC experiments were carried out on a VP-ITC (GE, Pittsburgh PA). Protein samples were buffer-exchanged to the desired buffer. Peptide concentration was prepared by adding buffer to the peptide powder as measured by weight. All samples were degassed 15-30 min before loading (GE MicroCal ThermoVac, Pittsburgh PA). To avoid buffer mismatch, the syringe and sample cells were rinsed with the desired buffer prior to sample loading. A typical titration was performed by sequential injections every 120-180 sec of 5-10

μL solution at 25°C, with a stir rate of 394 rpm. The ITC raw data was corrected for the heat of titrant dilution determined by an experiment conducted in identical conditions except that no protein was contained in the sample cell. The corrected data, after integration of heat evolved, was fitted with Origin software provided by the manufacturer to determine K_a and the observed or apparent ΔH (ΔH_{app}). For ANS (1-Anilinonaphthalene-8-Sulfonic acid) (Acros Organics) binding, a range of 5-50 μM CaM or chimera protein was titrated with 2-5 mM ANS solution in 30 mM HEPES, pH 7.5, 2 mM Ca^{2+}, with or without 0.1 M NaCl. The Orai-CMBD binding to the proteins was determined by titrating a solution of 1 mM Orai-CMBD in 10 mM Tris, pH 7.5, 2 mM Ca^{2+}, 0.1 M NaCl to 30 μM CaM or chimeras.

The possible buffer protonation/ionization to ΔH_{app} was determined using different buffers with known values of protonation enthalpy (ΔH_i).

$$\Delta H_{app} = \Delta H_b + n\Delta H_i \quad (1)$$

where n is the stoichiometry indicating how many protons are released or absorbed to the buffer. A positive sign of ΔH_i indicates a protonation process while a negative denotes a deprotonation process.

2.7 Spectroscopic Measurements

Absorption measurements were carried out using a UV-1800 double-beam spectrometer (Shimadzu, Kyoto, Japan). The fluorescence spectra were recorded on a FluoroMax-3P (Horiba John Yvon, Inc., Edison NJ) equipped with a temperature control unit. For intrinsic Trp fluorescence, the excitation wavelength of 295 nm was chosen. Note

that CaM and chimera proteins do not contain any Trp residues. The samples containing ANS or dansyl-labeled proteins were excited at 350 and 370 nm, respectively at 20ºC. The slit widths of 2 and 5 nm were typically chosen for excitation and emission, respectively, to eliminate photobleaching.

The fluorescence lifetime was measured with a TCSPC DeltaPro fluorometer (Horiba John Yvon, Inc., Edison NJ) at 20°C. For Trp lifetime measurements, a solution containing 15-20 μM Orai-CMBD with 5 μM protein was excited at 295 nm from a NanoLED295 source and the emission was detected with a 325 nm cutoff filter. For ANS lifetime measurements, each sample solution consisted of 5 μM CaM or chimera protein and 50 μM ANS in 30 mM Hepes, pH 7.5, 2 mM Ca^{2+} or 30 mM Hepes, pH 7.5, 2 mM Ca^{2+}, 0.1 M NaCl. The lifetimes of free and bound-ANS were determined separately with the excitation at 345 nm from a NanoLED350 light source and the emission with a 365 nm cutoff filter. The decay distorted by the instrument response was corrected with a "Prompt" measurement using 0.01% Ludox AS40 colloidal silica (Sigma-Aldrich). The time windows for Trp and ANS measurements were 100 and 200 ns in 4000 channels with 10,000 peak counts, respectively. The dynamic fluorescence decay was fitted with a multiple-exponential decay function as shown in Eq. 2, with the DAS6 software provided with the instrument. Only those data with a chi square (χ^2) value less than 1.2 were viewed as acceptable and reported.

$$I(t) = A + \sum_{i=1}^{n} \alpha_i e^{-t/\tau_i} \text{ and } f_i = \alpha_i \tau_1 / \sum_{i=1}^{n} \alpha_i \tau_i \text{ and } <\tau> = \sum_{i=1}^{n} \alpha_i \tau_i^2 / \sum_{i=1}^{n} \alpha_i \tau_i \qquad (2)$$

where I(t) is the fluorescence intensity at time t, α_i represents the pre-exponential factors, f_i is the fractional intensity, and $<\tau>$ is the amplitude-average lifetime.

The dissociation rate constant was obtained using a stopped-flow device (Hi-Tech Scientific SFA-20 Rapid Kinetics, TgK Scientific, UK). The peptide dissociation from CaM or chimeras was determined by mixing a solution containing 5 μM dansyl-CaM (or dansyl-labeled chimeras), 15 μM peptide, 2 mM Ca^{2+} with a solution containing 75 μM CaM and 2 mM Ca^{2+}. The solutions were excited at 370 nm and the signal changes at 497 nm (or 508 nm for CaM(1TnC) and CaM(2TnC) and 520 nm for CaM(3TnC) and CaM(4TnC)) were monitored. The integration and time intervals for all kinetic measurements were 2 and 5 ms, respectively. The dissociation was fit with the following exponential decay

$$Y = Y_o + A_o \exp(-(t-x_o)*k_{off}) \quad (3)$$

where Y is the observed fluorescence intensity at time t, Y_o and A_o are variables, x_o is the dead time and k_{off} is the dissociation rate constant.

2.8 Stern-Volmer Quenching

The Trp fluorescence quenching of the Orai-CMBD peptide was carried out at 20°C by adding stock solutions of 6 M acrylamide and 1 M KI to a sample solution containing CaM and peptide in 50 mM Tris, pH 7.5, 1 mM Ca^{2+}. The concentration of acrylamide was determined using the absorbance molar coefficient $\epsilon_{295} = 0.25\ M^{-1}\ cm^{-1}$. The concentration of peptide was 5 μM and the concentrations of proteins ranged from 20 to 40 μM to ensure no free peptide in the solution. The emission intensity was recorded at 350 nm for peptide only and at 330 nm for the complex. The following Stern-Volmer equation was used for fitting:

$$F_o/F = 1 + K_{SV}[Q] \quad (4)$$

where F and F_o are the fluorescence intensities at a given concentration of quencher ([Q]) and in the absence of quencher, respectively, and K_{SV} is the dynamic or collisional quenching constant.

For a quenching that is purely by collision, the steady-state and lifetime Stern-Volmer quenching equation can be expressed as

$$< \tau_o > / < \tau > \; = \; 1 + \; K_{sv}[Q] \text{ and } K_{sv} = k_q \text{ x } \tau_0 \quad (5)$$

where τ and τ_o are the lifetime in the presence and absence of the quencher, respectively, and k_q is the quenching rate constant.

2.9 Far-UV Circular Dichroism (CD)

The CD spectra were recorded in a JASCO J-715 instrument (JASCO Corporation, Japan) equipped with a temperature control unit. The system was purged with nitrogen for at least 30 min prior to use. CD spectra were recorded using a cylindrical 0.1 cm path length quartz cuvette and were shown as the average of 3-6 scans using a spectra bandwidth of 1.0 nm. In all measurements, 0.1 mg/mL proteins in 10 mM Tris, pH 7.5 with 1-2 mM Ca^{2+} or 0.5 mM EDTA were scanned from 190 nm to 260 nm. Scans with the Orai-CMBD complexes were performed in identical conditions, with the addition of 10-12 μM peptide, calculated based on the molar ratio obtained from ITC studies.

2.10 Modeling

The model structures of chimeras were generated and optimized with Swiss-Model Automatic Program Modeling Severs (http://swissmodel.expasy.org/) (Bordoli et al., 2009; Biasini et al., 2014) using 1CFC and 1CLL as the templates for apo and holo CaM forms, respectively. The modeling program uses the information from experimentally determined protein structures to generate a model for a target protein (i.e. chimera in our case). Briefly, the template (i.e. crystal structure of CaM) was selected to perform target/template alignment and the optimization for all-atom models for the target sequence using ProMol-II (Guex and Peitsch, 1997) or MODELLER (Sali and Blundell, 1993). Finally, the model was subjected to a model qualifying evaluation assigned by the local scoring function QMEAN. GETAREA was used to calculate solvent accessible surface areas (http://curie.utmb.edu/getarea.html) (Fraczkiewicz and Braun, 1998). The structures of Orai and chimera proteins were created in the same manner using the coordinates kindly provided by Dr. Birnbaumer (Liu et al., 2012). The electrostatic potentials were calculated using PyMol with Adaptive Poisson-Boltzmann Solver (APBS) plugin. First, a Poisson-Boltzmann calculation was performed using the PARSE force field in the PDB2PQR server (http://nbcr-222.ucsd.edu/pdb2pqr_1.8/) (Dolinsky et al., 2004). The resulting structure, containing charge and radius information, was used as an input for PyMol calculations. The following parameters were used for the calculation: 0.15 M for +1 and −1 ions, 310 K, 0.14 Å for solvent radius, and a dielectric constant of 2 and 78 for the protein and solvent, respectively.

CHAPTER 3

RESULTS AND DISCUSSION

3.1 Structural Change of CaM and Chimeras Probed with ANS

It is well known that the exposure of the hydrophobic patches of CaM is essential for target protein recognition. Such hydrophobic exposure can be photometrically monitored by its interaction with extrinsic 1-anilinonaphthalene 8-sulfonate (ANS) and 2-p-Toluidinyl-naphthalene-6-sulfonate (TNS) molecules. These two fluorophores have been widely used as a probe for measuring hydrophobicity. ANS is a fluorescent dye which emits very weak fluorescence in water due to its excited charge transfer (CT) state that is quenched easily by water molecules. ANS alone exhibits very little fluorescence with a maximal wavelength (λ_{max}) of 520 nm (Figure 8). ANS fluorescence increases dramatically in a hydrophobic environment or when the rotational motion of its phenylamino group is restricted (Someya and Yui, 2010). In the absence of Ca^{2+}, the ANS fluorescence of CaM or chimeras exhibited no change, mainly due to the lack of hydrophobic surface and the presence of electrostatic repulsion between the negatively charged sulfonate group of ANS and the negatively charged residues in CaM and chimeras. The fluorescence increased when Ca^{2+} was included in the mixture. The ANS intensity showed a 3.01 ± 0.12 fold increase (Table 1; fold increase was determined by the integration of the whole spectrum and all following values are referred to in the same manner) and λ_{max} was blue shifted from 520 to 480 nm in our experimental conditions. This observation is consistent with the fact that the Ca^{2+}-bound CaM (Ca^{2+}-CaM) exposes its hydrophobic surface, followed by ANS binding, in which the protein-bound ANS molecules are more shielded from the solvent. ANS intensity

enhancements were also observed in all Ca^{2+}-chimeras, with identical concentrations of the protein and dye, exhibiting increases in fluorescence ranging from 1.56-2.72 fold (Table 1). Our results appear to suggest that the chimeras have less hydrophobic surface exposure compared with CaM, consistent with the fact that there is no interaction between TnC and ANS (Fidalgo Da Silva et al., 2006). However, such a conclusion does not provide instructive information because it is unclear on whether the ANS enhancements were due to an increase in ANS lifetime (or quantum yield) and/or binding affinity. Thus, we turned to study CaM/chimera ANS binding by using isothermal titration calorimetry (ITC) and lifetime fluorescence.

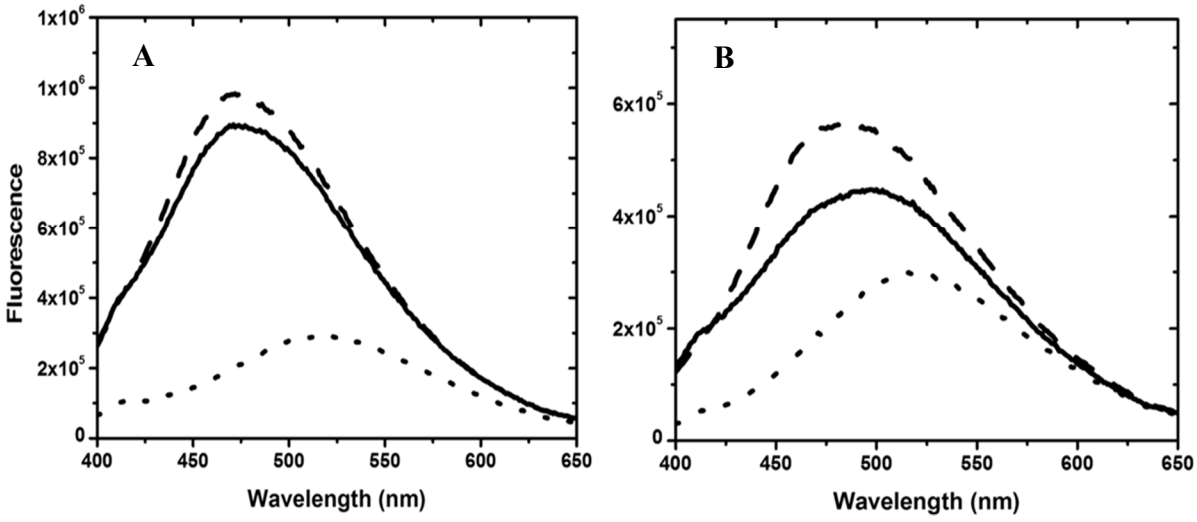

Figure 8: ANS fluorescence of uncomplexed and complexed CaM and CaM(3TnC). (A) shows the ANS fluorescence of a solution containing 200 μM ANS and 5 μM CaM in the absence (dotted line) and presence (solid line) of Ca^{2+}. The ANS fluorescence of CaM/Orai-CMBD was recorded by adding a solution of Orai peptide into Ca^{2+}-CaM until no more intensity change was observed (dashed line). **(B)** shows the ANS fluorescence of CaM(3TnC) in identical experimental conditions as in **(A)**. ANS fluorescence was excited at 350 nm.

The raw ITC data for ANS binding to CaM is shown in Figure 9. The initial ANS injections resulted in heat released from the complex as shown in a downward heat rate. The heat evolved is proportional to the amount of the ANS/Ca^{2+}-CaM complex formation. Apparently, the titration did not reach completion due to the weak ANS binding. We fit the data with "one set of sites" to obtain the apparent association binding constant (K_{app}) of $2.10 \pm 0.11 \times 10^3$ M^{-1} for Ca^{2+}-CaM (Table 1), consistent with a previous report (Yamniuk et al., 2009). Note that K_{app} is not the binding constant for the ANS molecule; rather it represents the overall low-affinity interaction of the multiple ANS molecules to CaM. It is unclear how many ANS binding sites exist in CaM, given a range of 2-5 ANS molecules in CaM complexes have been reported (Suko et al., 1985; Moorthy et al., 1999). Based on our studies, the middle point from the ITC thermogram (and the inflection point in the corresponding derived binding isotherm) indicates approximately 4-6 bound-ANS molecules in Ca^{2+}-CaM. Therefore, K_{app} is proportional to the actual number of protein-bound ANS molecules in the experimental condition. In the text below, we will discuss K_{app} as the ANS binding affinity for simplicity. Almost all chimera proteins, except CaM(4TnC), showed a significant lower ANS binding affinity, which is parallel to the findings from fluorescence (Table 1). For example, CaM(3TnC) has the lowest ANS fluorescent enhancement (1.56 ± 0.04 fold) and binding constant ($6.70 \pm 0.51 \times 10^2$ M^{-1}). In the presence of 0.1 M NaCl, both the ANS fluorescence enhancements and association binding constants for CaM and chimera proteins increased (Table 1), indicating that the salt screens the repulsion between ANS and the acidic residues in the proteins. In the absence of Ca^{2+}, no ANS binding was observed in the ITC experiments, consistent with the fluorescence studies.

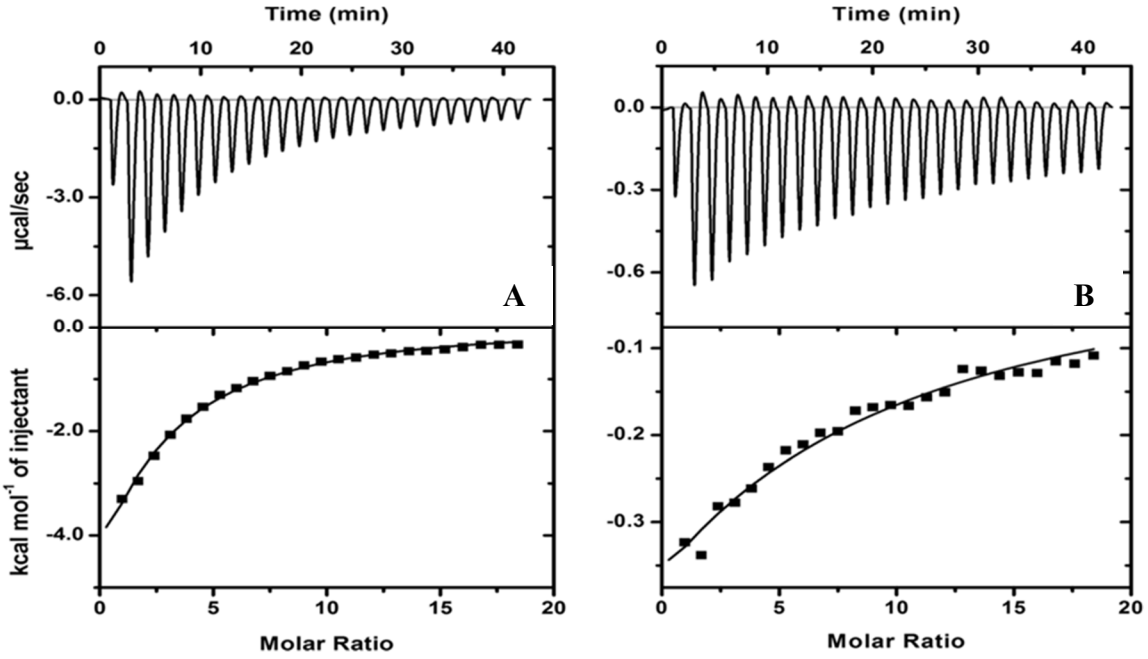

Figure 9: ANS binding to CaM and CaM(3TnC) by isothermal titration calorimetry. A solution of 50 µM CaM **(A)** or CaM(3TnC) **(B)** were titrated with 5 mM ANS at 25°C in the presence of Ca^{2+}. The ITC data were fit with a "one set of sites" model as described in the Experimental section. The values from the fitting are shown in Table 1.

Table 1: ANS binding to CaM and chimeras by fluorescence and ITC

	ANS binding in the absence of salt		ANS binding in the presence of salt		ANS binding in the presence of salt and Orai-CMBD	
Protein	**ANS enhancement (fold)[a]**	**K_{app} (10^3 M^{-1})**	**ANS enhancement (fold)[a]**	**K_{app} (10^3 M^{-1})**	**ANS enhancement (fold)[a]**	**K_{app} (10^3 M^{-1})**
CaM	3.01 ± 0.12	2.10 ± 0.11	3.49 ± 0.07	3.69 ± 0.08	3.87 ± 0.10	3.43 ± 0.65
CaM(1TnC)	2.72 ± 0.10	0.99 ± 0.12	3.33 ± 0.06	1.13 ± 0.04	3.31 ± 0.05	1.20 ± 0.08
CaM(2TnC)	2.55 ± 0.05	1.01 ± 0.07	3.01 ± 0.14	1.10 ± 0.01	3.07 ± 0.04	9.70 ± 0.31
CaM(3TnC)	1.56 ± 0.04	0.67 ± 0.51	1.74 ± 0.08	0.86 ± 0.21	2.24 ± 0.11	1.07 ± 0.10
CaM(4TnC)	2.37 ± 0.22	1.80 ± 0.05	2.90 ± 0.19	2.02 ± 0.03	3.62 ± 0.15	2.67 ± 0.24

[a]The ANS intensity enhancements were calculated from spectra integration and compared to the corresponding apo proteins in identical experimental conditions.

Given that steady state fluorescence cannot differentiate the intensity contribution from individual ANS molecules, we utilized time-correlated single-photon counting (TCSPC) spectrometry to measure the ANS fluorescence decay. A solution of 5 µM CaM

and 50 μM ANS in the presence of 2 mM Ca^{2+} was excited with a 345 nm light source from a NanoLED and the emission was monitored with a 365 nm cutoff filter. The decay and the fitted function are shown in Figure 10. The data was best fit with a three-exponential-decay function. The shortest lifetime (τ_3 = ~0.3 ns) was assigned to that of free ANS molecules (Robinson et al, 1978), which was confirmed by using an ANS solution alone. Note that this lifetime reaches the detection limitation of our instrument and therefore, it cannot be determined precisely. Two longer lifetimes, τ_1 = 6.4 and τ_2 = 13.1 ns, were only observed in the presence of Ca^{2+}, thus suggesting two different ANS populations with rather different probe environments. The fitting also provided the fractional (or relative amplitude), f_s, which weights the "amount" of the emitting species, and the normalized pre-exponential value, B_s, which provides the relative concentration of each species. The data for Ca^{2+}-CaM indicates that the τ_1 and τ_2 species contribute more than 95 % (i.e. $f_1 + f_2$) to the fluorescence intensity, but consist of less than 30% of the total species (i.e. $B_1 + B_2$). When decreasing the [ANS]/[CaM] ratio from 10 to 0.5, the fluorescence intensity is attributed to high "relative concentrations" of the two longer lifetimes, with f_1 = 0.47, B_1 = 0.33 and f_2 = 0.49, B_2 = 0.16. Double fluorescence lifetime of bound-ANS (or ANS heterogeneity) is commonly seen in proteins (D'Alfonso et al., 1999) and in molten globular structures (Uversky et al., 1996), where the later showed that ANS has τ_1 = ~2 ns and τ_2 = ~6 ns, in which the short lifetime represents ANS molecules located on the protein surface, while the longer lifetime represents ANS in the protein matrix. The data shown here indicates that the CaM-bound ANS molecules are located in a very hydrophobic environment, limiting its solvent accessibility capacity. In fact, the Stern-Volmer quenching by acrylamide (see experimental section) revealed a linear decrease in two lifetime components, yielding K_{SV} values for the short and

long lifetime ($K_{SV}(\tau_1)$ and $K_{SV}(\tau_2)$) of 1.4 ± 0.2 M^{-1} and 0.25 ± 0.05 M^{-1}, respectively. The quenching rate constant (k_q) for ANS with the short lifetime is 2.2 x 10^8 M^{-1} s^{-1} while k_q for τ_2 is 1.9 x 10^7 M^{-1} s^{-1}, indicating the latter is less solvent accessible. In other words, the long lifetime component of ANS is one order less quenched by acrylamide.

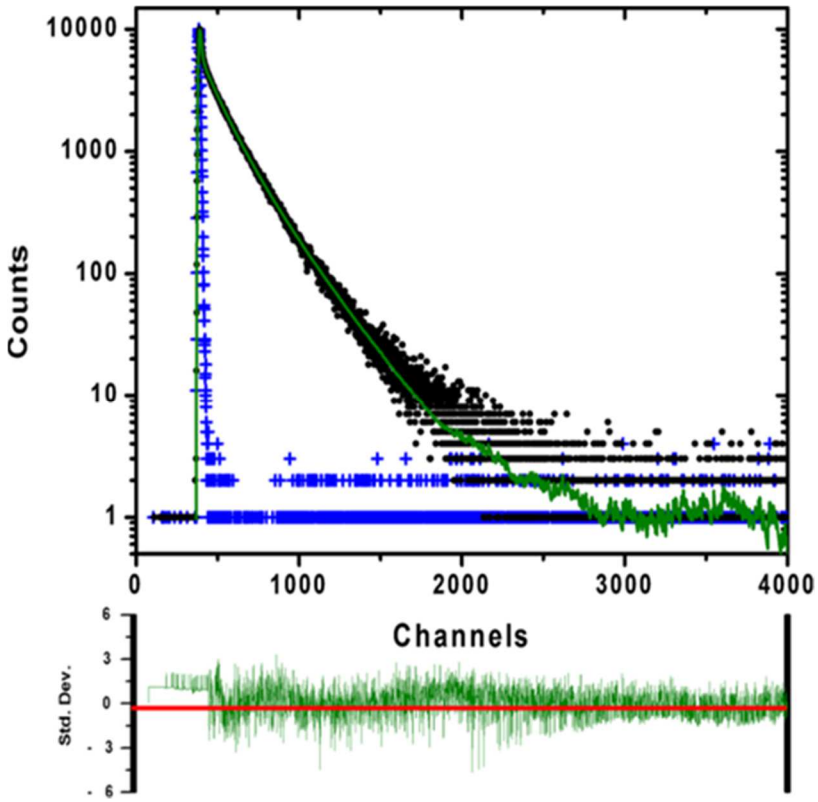

Figure 10: The lifetime measurement of CaM-bound ANS. A solution containing 5 μM CaM and 50 μM ANS was excited with 345 nm from a NanoLED light source and its dynamic fluorescence decay (black) was monitored with TCSPC using a 200-ns window for 4000 channels. The prompt is shown in blue color. The decay was best fitted with a three-exponential decay (green line in upper panel) and the weighted residues are indicated in the lower panel. The calculated χ^2 is 0.986. The values from the fitting are shown in Table 2.

It is unclear where the binding sites of the ANS molecules are located in CaM. Using the fragments from the tryptic cleavage of CaM, it has been suggested that two ANS molecules bind to the N- and C-terminal lobes (Suko et al., 1985). However, the summation

of ANS fluorescence from individual lobes is much less than that of the intact CaM. Therefore, we believe that there are multiple ANS binding sites for CaM, but only two types are distinguishable from each other based on the lifetime measurements. We expected that the interaction of chimeras and ANS might affect the lifetime and/or its population (thus contributing to different f values). Such information cannot only be used to correlate with steady-state fluorescence, but also may provide information about the individual lobes.

The lifetimes of CaM(1TnC)- and CaM(2TnC)-bound ANS molecules are different compared to those of CaM, with a similar τ_1 value but substantially larger τ_2 value (~18 ns). The exchanged EF-hands in the N-terminal lobes appear to reflect a longer ANS lifetime. On the other hand, τ_1 for CaM(3TnC) and CaM(4TnC) is smaller than that of CaM while their τ_2 is similar to that of CaM, indicating the exchanged EF3 and EF4 have a less profound impact on the ANS short lifetime component. The average lifetime ($<\tau>$) calculated from Eq. 2 for each chimera is displayed in Table 2, showing CaM(1TnC) and CaM2(TnC) have a significant longer ANS average lifetime (13-14 ns). Though a longer lifetime observed in CaM(1TnC) and CaM(2TnC) should attribute to a higher fluorescence intensity, such a contribution is shaded by the weaker binding as indicated by the ITC studies.

Table 2: ANS lifetime[a] for the uncomplexed and complexed CaM and chimeras

	Without Orai-CMBD					With Orai-CMBD				
	Component 1		Component 2		Average	Component 1		Component 2		Average
	τ_1 (ns)	f_1	τ_2 (ns)	f_2	$<\tau>$ (ns)	τ_1 (ns)	f_1	τ_2 (ns)	f_2	$<\tau>$ (ns)
Ca^{2+}-CaM	6.4	0.44	13.1	0.53	9.0	6.8	0.20	16.9	0.66	13.1
Ca^{2+}-CaM(1TnC)	6.2	0.21	17.8	0.70	14.4	6.3	0.31	17.3	0.57	12.7
Ca^{2+}-CaM(2TnC)	5.9	0.20	17.7	0.68	13.7	5.8	0.18	17.3	0.71	12.9
Ca^{2+}-CaM(3TnC)	4.4	0.29	12.1	0.51	7.4	4.3	0.30	16.2	0.57	11.7
Ca^{2+}-CaM(4TnC)	5.1	0.19	12.9	0.70	8.6	6.0	0.16	17.1	0.72	13.5

[a]Data from the fitting are shown as an average for clarity.

In summary, we observed a correlation between K_{app} values and fluorescence enhancements for ANS binding, which is on the order of CaM > CaM(1TnC) ~ = CaM(2TnC) > CaM(3TnC). The lower fluorescence enhancements observed in chimera proteins are dominated by a lower ANS binding affinity. The lifetime measurements also revealed ANS heterogeneity. The exchanged EF-hands appear to alter ANS lifetimes and fractional values (i.e. molecule population), with the exchanged EF-hands in the N-terminal lobe likely to increase the longer lifetime component while those in the C-terminal lobe are likely to slightly decrease the short lifetime component. CaM(4TnC) is the exception to the trend, with the second lowest in ANS fluorescence enhancement but the second highest ANS binding affinity. Here, the ANS fluorescence decrease due to the shorter lifetime (5.1 ns) is compensated by a higher ANS binding affinity ($1.80 \pm 0.05 \times 10^3$ M^{-1}). If ANS fluorescence of a protein truly reflects the hydrophobic area of the protein, then our data supports the previous reports that replacing CaM's EF-hands with those of TnC results in a lower ability to expose hydrophobic surface area (Fidalgo Da Silva et al., 2006). However, the extent of hydrophobicity determined from steady-state ANS fluorescence can be misleading, as it both over and underestimated ANS binding in the CaM/TnC system determined from ITC.

3.2 Fluorescence Studies Reveal the Ca^{2+}-Dependent Interaction between Orai Peptide and CaM Derivatives

We then studied how CaM and the chimeras interact with a synthetic 24 amino acid peptide corresponding to the CaM-binding domain of an Orai channel protein (Orai-CMBD). Since Orai-CMBD contains a Trp76 residue (numbering in Orai) and there are no Trp

residues in CaM, Trp fluorescence can be used to investigate the interaction between Orai-CMBD and CaM. The excitation wavelength at 295 nm was chosen to eliminate the signal from CaM's Tyr residues. The peptide alone exhibited low fluorescence with λ_{max} of 350 nm in a Ca^{2+}-independent manner. Upon the addition of Ca^{2+}-CaM, Trp fluorescence was enhanced 1.82 fold and λ_{max} was blue-shifted from 350 to 335 nm, suggesting that the Trp76 is embedded in a more hydrophobic environment provided by CaM (Figure 11). In an identical experiment but without Ca^{2+}, no major signal change was observed upon the addition of CaM, supporting the conclusion that the interaction between Orai and CaM is Ca^{2+}-dependent. The chimera proteins revealed a similar Trp fluorescence change with the trend of CaM > CaM(4TnC) = CaM(3TnC) > CaM(1TnC) > CaM (2TnC) (Table 3). The small difference in intensity change and λ_{max} suggests Trp76 is bound within the proteins in a similar manner.

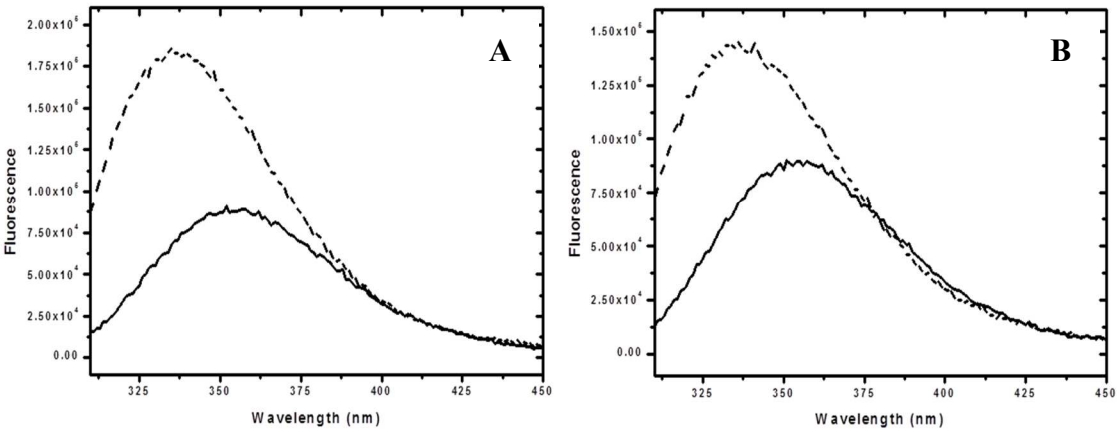

Figure 11: Trp76 Orai-CMBD fluorescence of CaM and CaM(2TnC). (A) shows the intrinsic Trp fluorescence of Orai-CMBD peptide alone (solid line) and following excess Ca^{2+}-CaM addition (dotted line). **(B)** shows the intrinsic Trp fluorescence of Orai-CMBD complexed with Ca^{2+}-CaM(2TnC) in identical experimental conditions as in **(A)**.

The interaction of Orai-CMBD to Ca^{2+}-CaM can also be monitored using ANS fluorescence. In the absence of Orai-CMBD, Ca^{2+}-CaM and Ca^{2+}-chimeras interact with ANS differently with λ_{max} = 480 nm for CaM, CaM(1TnC), and CaM(2TnC) and λ_{max} = 500 nm for CaM(3TnC) and CaM(4TnC) (Figure 8). The Orai-CMBD binding to CaM enhanced ANS fluorescence ~10%, mainly due to the resulting increases in lifetime (Table 2) but not affinity (Table 1). Orai-CMBD binding to CaM retains a similar short ANS lifetime (i.e. 6.4 versus 6.8 ns) but increases the long lifetime from 13.1 to 16.9 ns, respectively (Table 2), whereas Orai-CMBD binding to CaM(1TnC) and CaM(2TnC) neither increased ANS intensity enhancements, lifetime, and binding affinity. Orai-CMBD binding to CaM(3TnC) and CaM(4TnC) restored their λ_{max} from 500 to 480 nm and increased ANS intensities ~30% and 25%, respectively (Table 1). The fluorescence enhancement was primarily due to the increase in both lifetime and binding affinity. Our data revealed that exchanging an EF-hand in the same lobe (N- or C-terminal) exhibits a similar structural effect probed by the ANS molecule, consistent with the functional dependency of a tandem EF-hand pair in most EF-hand containing proteins.

The non-significant change of ANS lifetimes in the N-terminal lobes of CaM(1TnC) and CaM(2TnC) suggests that peptide binding causes either minimal conformational change on that lobe or a structural change not sensitive to the ANS probe. On the other hand, CaM(3TnC) and CaM(4TnC) have a very similar response to that of CaM, suggesting the exchanged EF-hands in the C-terminal end retain their ability of conformational change for peptide binding.

3.3 Stern-Volmer Quenching to Determine the Solvent Accessibility of Trp76

To investigate the microenvironment of Trp76 of Orai-CMBD, we employed collision quenching of Trp fluorescence by determining the accessibility of Trp residues to acrylamide and potassium iodide (KI) for the free and CaM-bound forms of Orai-CMBD. These two quencher molecules diffuse differently into the protein pocket and thus provide different environmental information for Trp. Fluorescence quenching is the result of Trp either being translocated to the surface of the protein, or Trp being located within the protein interior which allows acrylamide to diffuse into hydrophobic pockets. When Trp is flanked by positively charged residues, the quenching becomes more effective with the use of an anionic quencher such as I^-. In the conditions employed, the amounts of CaM and chimeras were added in excess (based on the molar ratio determined from ITC) to ensure that there was no free peptide in the solution. We only observed a linear quenching curve in Trp quenching at the concentrations used for acrylamide and KI (Figure 12). Orai-CMBD alone showed that its Trp residue was greatly accessible for quenching by acrylamide (K_{sv} = 13.5 ± 0.4 M^{-1}) and KI (K_{sv} = 13.1 ± 0.5 M^{-1}) (Table 3). It is not surprising that the Ca^{2+}-CaM binding to Orai-CMBD rendered protection against Trp quenching with either acrylamide (K_{sv} = 1.35 ± 0.08 M^{-1}) or KI (K_{sv} = 1.31 ± 0.08 M^{-1}). The quenching studies were further extended by lifetime measurements. The fluorescence decay of Trp in Orai-CMBD, excited at 295 nm and monitored by a 325 nm cutoff filter, was best fit with a three-exponential-decay function with τ_1 = 0.29, τ_2 = 3.1 and τ_3 = 7.5 ns, which is consistent to a complex lifetime observed for Trp in proteins. The addition of Ca^{2+}-CaM to the Orai-CMBD solution increases the fractions, f_2 and f_3, for τ_2 and τ_3 significantly, but no information could be obtained about binding stoichiometry due to the complex Trp lifetime.

Since the determination for τ_1 is within the detection limitation of our TCSPC and its contribution to the overall fluorescence decay is negligible, we excluded it from quenching analysis. As shown in the insert of Figure 12, the τ_2 and τ_3 components both were quenched, but to a different extent. The K_{sv} for the longer lifetime τ_2 ($K_{sv}(\tau_2)$) is 1.52 M^{-1} and $K_{sv}(\tau_3)$ is 0.90 M^{-1}. Since the steady-state K_{sv} is between the two K_{sv} values obtained from the lifetime measurement, it indicates that the quenching is a dynamic collision, not a static model. The lifetime quenching by KI exhibited similar results to those obtained by acrylamide.

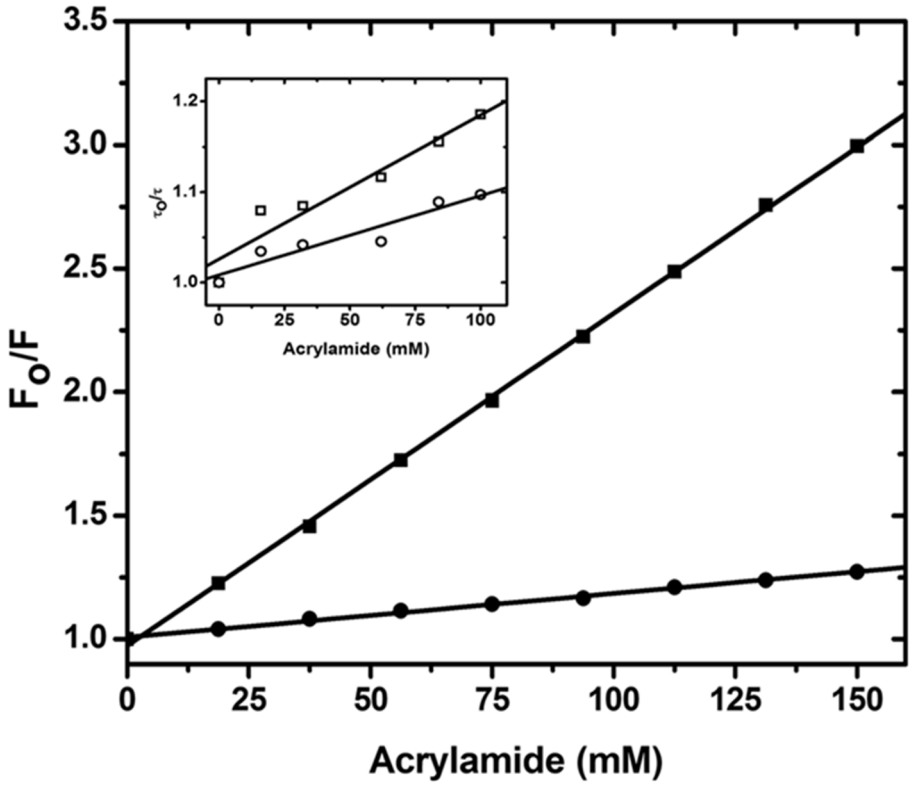

Figure 12: Stern-Volmer plot of Trp76 fluorescence of Orai-CMBD quenched by acrylamide. A representative figure of Stern-Volmer quenching by acrylamide is shown for Orai-CMBD and CaM/Orai-CMBD based on steady state fluorescence. To ensure no free Orai-CMBD peptide in the complex, CaM or the chimeras were added into the solution of 5 μM Orai-CMBD until no significant fluorescence change was observed. The values from the fitting are shown in Table 3. **Insert:** the quenching was monitored by two lifetime components of Trp76 of Orai-CMBD in the complex.

Upon repeating similar studies using the chimera proteins, the Trp fluorescence in the complex with CaM(1TnC) and CaM(2TnC) was slightly more solvent accessible than CaM, while CaM(3TnC) and CaM(4TnC) displayed similar quenching values to those of CaM (Table 3). Surprisingly, the Stern-Volmer values obtained from KI are very comparable to those from acrylamide studies, suggesting that the Trp76 of Orai-CMBD is embedded very deeply in a hydrophobic environment, such that the size and charged state of the quenchers cannot be used to differentiate the microenvironment. Our data aligns with the crystal structure, showing that Trp76 of Orai-CMBD is surrounded by several hydrophobic residues.

Table 3: Trp76 of Orai-CMBD fluorescence and Stern-Volmer quenching constants

Protein	λ_{max} (nm)	Trp fluorescence enhancement upon protein binding (fold)	K_{sv} (M^{-1}) acrylamide	K_{sv} (M^{-1}) KI
Orai-CMBD	350	n.a.	13.5 ± 0.4	13.1 ± 0.5
Ca^{2+}-CaM/Orai-CMBD	335	1.82 ± 0.06	1.35 ± 0.08	1.31 ± 0.08
Ca^{2+}-(CaM)1TnC/Orai-CMBD	335	1.61 ± 0.05	1.80 ± 0.09	1.75 ± 0.06
Ca^{2+}-(CaM)2TnC/Orai-CMBD	336	1.44 ± 0.11	1.95 ± 0.10	1.85 ± 0.05
Ca^{2+}-(CaM)3TnC/Orai-CMBD	336	1.75 ± 0.08	1.32 ± 0.05	1.21 ± 0.09
Ca^{2+}-(CaM)4TnC/Orai-CMBD	337	1.76 ± 0.07	1.51 ± 0.04	1.22 ± 0.10

3.4 Thermodynamics of Orai-CMBD to CaM and Chimeras

The data from fluorescent studies indicated that the individual exchanged EF-hands alter the surface hydrophobicity but retain the binding to Orai-CMBD. However, it is unclear about the specifics of such an interaction. Thus, we used ITC to obtain the thermodynamics of Orai-CMBD to CaM and chimeras. The Orai-CMBD titration to CaM in the presence of Ca^{2+} at 25°C exhibited a typical calorimetric reaction (Figure 13A upper panel), in which the heat release per injection was observed. The heat evolved decreased gradually until the background signal was reached. The plot of heat evolved per injection (ΔQ_i) versus molar

ratio showed an exothermic, sigmoid-shape binding isotherm (Figure 13A lower panel). The ITC data was best fit into a "one set of sites" model and the K_a and ΔH values were determined to be $8.92 \pm 1.03 \times 10^5$ M^{-1} and -5.02 ± 0.13 kcal/mol, respectively, with N = ~2 (Table 4). The data agreed with the previous report (Liu et al., 2012) and indicates that CaM contains two Orai-CMBD binding sites, each with a similar binding affinity and enthalpy change that are not distinguishable with the calorimetric measurement.

The ITC measurements provide information about net non-covalent interactions, including hydrogen bonds, ionic interactions, and van der Waals (VDW) interactions, as well as water solvation. However, proton release or uptake from solvent in the formation of a complex may contribute significantly to the apparent determined enthalpy (ΔH_{app}). Therefore, the heat evolved due to buffer protonation/ionization has to be determined and corrected to obtain accurate binding information. Using different buffers, including HEPES, Tris, and POPS, we found no significant ΔH_{app} change. Therefore, we concluded that there was no significant protonation in the CaM/Orai-CMBD complex, in which the obtained enthalpy difference becomes the binding enthalpy (ΔH_b). We then performed similar experiments using the chimera proteins. The ITC raw data and thermogram of CaM(1TnC) and CaM(2TnC) clearly cannot be interpreted with a "one set of sites" binding model (Figure 13B). It appears that the binding consists of a tighter binding with a higher ΔH_b followed by a weaker binding with a lower ΔH_b. The ITC data of CaM(1TnC) can be best fit with a two sequential binding mode, yielding $K_{a1} = 7.57 \pm 1.10 \times 10^5$ M^{-1}, $\Delta H_{b1} = -4.99 \pm 0.14$ kcal/mol and $K_{a2} = 1.70 \pm 0.30 \times 10^4$ M^{-1}, $\Delta H_{b1} = -3.33 \pm 0.30$ kcal/mol. Because K_{a1} and ΔH_{b1} are close to that of CaM, those values are assigned to Orai-CMBD binding to the C-terminal lobe of CaM while the lower binding K_{a2} and the lower ΔH_{b2} are associated with

the N-terminal lobe of the chimeras. This conclusion was further supported by the data from CaM(2TnC), which displayed a similar binding event as CaM(1TnC). Interestingly, the binding affinity and enthalpy change for Orai-CMBD complexed with CaM(3TnC) and CaM(4TnC) are comparable to those of CaM, suggesting that the impact from the exchanged EF3 and EF4 are less important for the binding. On the other hand, the exchange of EF1 and EF2 resulted in a one-order weaker binding affinity and a lower enthalpy change. Although it is a challenge to interpret the structural changes from the obtained thermodynamic parameters, our result still provides insights for the binding. The negative ΔH_b values present the non-covalent bond energy for the complex formation while the positive entropy change, ΔS, reflects the entropic gain associated with desolvation, as seen in hydrophobic interactions. For CaM/Orai-CMBD, the driving force for the reaction is both enthalpic and entropic given the negative ΔH_b and positive ΔS (~10 cal/mol·K calculated from $\Delta G = \Delta H - T\Delta S$ and $\Delta G = -RT\ln(K_a)$ where ΔG is the free energy change and T is temperature). Our data also showed that the exchange of EF1 and EF2 in CaM(1TnC) and CaM(2TnC) either formed significantly fewer non-covalent interactions and/or impaired the side chain packing and dynamics upon complex formation. It is very surprising to us that the hydrophobic surface probed by ANS does not correlate with Orai-CMBD binding given that CaM(3TnC) had the lowest ANS fluorescence but a comparable binding to Orai-CMBD. This contradicts the general concept that the hydrophobicity assessed by ANS reflects the actual extent of hydrophobic exposure.

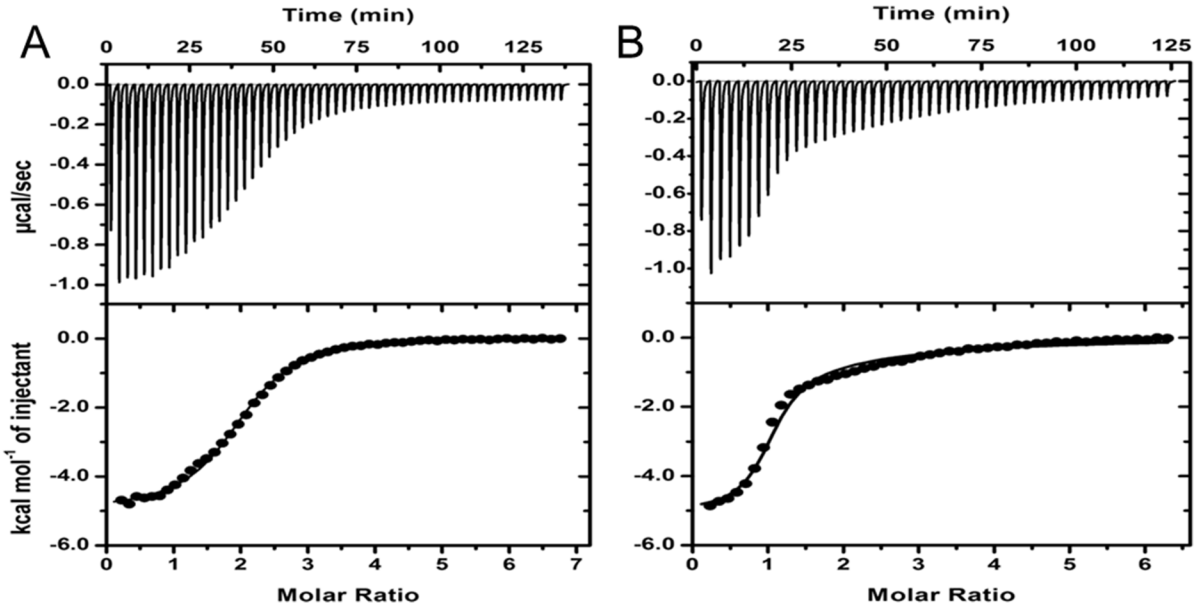

Figure 13: The binding thermodynamics of Orai-CMBD to CaM and CaM(1TnC) determined by ITC. A solution of 30 µM CaM **(A)** or CaM(1TnC) **(B)** was titrated with 1 mM Orai-CMBD in 10 mM Tris, pH 7.5, 0.1 M NaCl, 2 mM Ca^{2+}. The upper panels show the heat evolved per injection and the lower panels show the integrated heat per injection versus the molar ratio. The model for the fitting was "one set of sites" for CaM and two sequential binding sites for CaM(1TnC). In both cases, the middle points of the thermograms indicates a stoichiometry of 1:2 protein:ligand binding. The values from the fitting are shown in Table 4.

3.5 Kinetics of Orai-CMBD to CaM and Chimeras

To study the kinetics of Orai-CMBD associated or dissociated from CaM, we used a stopped-flow device to determine the association and dissociation rate constants, k_{on} and k_{off}, respectively. The association was initiated by quickly mixing the Ca^{2+}-CaM and Orai-CMBD solutions in the presence of Ca^{2+} and determined by its fluorescence, excited and monitored at 295 nm and 330 nm, respectively. Like other CaM/CMBD systems, k_{on} was too fast to be observed (Kleerekoper and Putkey, 2009). Orai-CMBD release from Ca^{2+}-CaM was triggered by mixing a solution containing 5 µM dansyl-labeled CaM (dansyl-CaM) and an excess of Orai-CMBD with a solution containing 75 µM unlabeled CaM in the presence of Ca^{2+}. The fluorescence of Ca^{2+}-dansyl-CaM has a λ_{max} at 520 nm when excited at 370 nm.

The Orai-CMBD binding resulted in a fluorescence increase and a λ_{max} blue shift to 490 nm. In the stopped-flow, the Orai-CMBD release from dansyl-CaM after mixing was promptly trapped by CaM, resulting in a dansyl fluorescence decrease (Figure 14A). The decay was best fit with a single exponential equation (Eq. 3) giving k_{off} = 1.41 ± 0.08 s^{-1} (Table 4). Using the dansyl-labeled CaM(1TnC) and CaM(2TnC), the k_{off} values were determined to be 2.44 ± 0.21 and 2.64 ± 0.32 s^{-1}, respectively (Figure 14B and Table 4). The peptide dissociation rates appear to be two-times slower for CaM(3TnC) and CaM(4TnC) (Figure 14C and Table 4). It is noteworthy to mention that only a single exponential decay was observed in all cases. Given that it is generally accepted that the two lobes of CaM function independently, we expected that either there would be two distinct k_{off} values exhibited for the chimeras if the kinetics are different for individual lobes, or a single k_{off} value (as seen in CaM) that reflects the Orai-CMBD dissociation from a specific lobe. It has been reported that the dansyl-labeling occurs in a single domain of CaM (Kincaid et al., 1982) and it is also suggested that the labeling site is near the N-terminal lobe (Matsubara et al., 1997). If this is the case, then the obtained k_{off} values presented the Orai-CMBD dissociation kinetics specifically at the N-terminal lobe. This indicates that the lower ligand binding affinity (i.e. K_{a2}) seen in the N-terminal lobe of CaM(1TnC) and CaM(2TnC) is partly due to the fast ligand dissociation rate. However, such an explanation cannot be applied to CaM(3TnC) and CaM(4TnC), in which the k_{off} values should be similar to that of CaM, if assuming an identical dansyl-labeled site. It is possible that our labeling in the exchanged EF3 and EF4 proteins exists within the other lobe given the very different dansyl fluorescence seen in CaM(3TnC) and CaM(4TnC). Thus, the slower ligand dissociation rate may be associated with the C-terminal lobe.

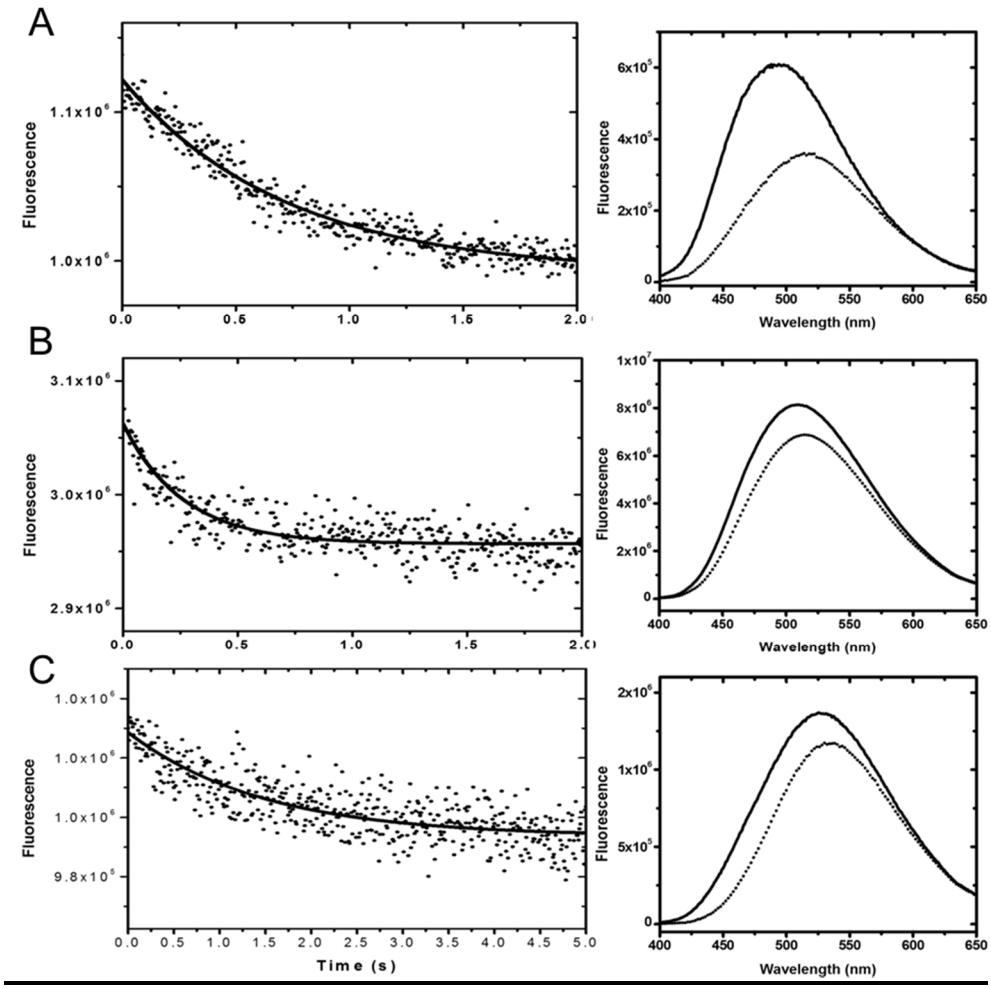

Figure 14: Kinetics of Orai-CMBD to CaM and chimeras. A solution of 5 μM dansyl-CaM, dansyl-CaM(1TnC), or dansyl-CaM(3TnC) and 15 μM Orai-CMBD was quickly mixed with a solution containing 75 μM CaM in the presence of 2 mM Ca^{2+} and the fluorescence decay was monitored for 2 sec for CaM **(A)** and CaM(1TnC) **(B)** and 5 sec for CaM(3TnC) **(C)** (left panel). The decay was fitted with a single exponential decay and the resulting k_{off} values are shown in Table 4. The peptide dissociated from dansyl-CaM or chimeras from the mixing resulted in the intensity decrease as observed in the complexed and uncomplexed fluorescently labeled CaM or chimeras (right panel).

Table 4: Thermodynamics and kinetics of Orai-CMBD to CaM and chimeras

Protein	K_{a1} (10^5 M^{-1})	ΔH_1 (kcal/mol)	K_{a2} (10^4 M^{-1})	ΔH_2 (kcal/mol)	Binding model or N for one-site	k_{off} (s^{-1})
CaM	8.92 ± 1.03	- 5.02 ± 0.13	n.a.	n.a.	N = 2.05 ± 0.30	1.41 ± 0.08
CaM(1TnC)	7.57 ± 1.10	- 4.99 ± 0.14	1.70 ± 0.30	- 3.33 ± 0.30	Sequential	2.44 ± 0.21
CaM(2TnC)	6.66 ± 0.20	- 5.21 ± 0.21	1.39 ± 0.35	- 3.79 ± 0.39	Sequential	2.64 ± 0.32
CaM(3TnC)	2.90 ± 0.12	- 6.58 ± 0.05	n.a.	n.a.	N = 1.93 ± 0.24	0.68 ± 0.25
CaM(4TnC)	5.77 ± 1.35	- 5.34 ± 0.40	n.a.	n.a.	N= 1.87 ± 0.15	0.72 ± 0.31

3.6 Circular Dichroism to Monitor Secondary Structure Changes

We used circular dichroism (CD) to monitor the secondary structure of Ca^{2+}-CaM upon Orai-CMBD binding. Ca^{2+}-free CaM showed a shape typical of an α-helical structure with a negative peak (ellipticity or θ) at 220 nm and a more profound negative peak 209 nm. Ca^{2+} binding induced additional α-helical formation in CaM and chimeras, which showed relatively equal intensities at 220 and 209 nm. Because θ_{220} presents more closely to the α-helical content, whereas θ_{209} contributes more significantly from the β sheet and random coil structure, the ellipticity ratio at these two wavelengths (i.e. $\theta_{220}/\theta_{209}$) indicates the secondary structural change relative to the α-helix content. A perfect helix peptide or a protein with all helix structure has a $\theta_{220}/\theta_{209}$ value of 1.09. Ca^{2+}-CaM contains α-helix content ranging from 45-60% in solution (Martin and Bayley, 1986) and crystal structures (Babu et al., 1985). The ellipticity ratio for Ca^{2+}-CaM is approximately 1 due to the coil structure that exhibits a large negative ellipticity at 198 nm and slightly positive ellipticity at 205 nm. No significant change in the ellipticity ratio was observed for CaM(1TnC) and CaM(2TnC), however slightly less α-helical content was induced upon Ca^{2+}-binding for CaM(3TnC) and CaM(4TnC) in relation to CaM (Table 5).

The CD spectrum of Ca^{2+}-CaM/Orai-CMBD shifted to a more negative value at 220 and 209 nm, giving a $\theta_{220}/\theta_{209}$ value of 0.89 indicating significant structural changes for the complex formation. Given that there is no significant change observed in the uncomplexed and complexed CaM (Meador et al., 1992; Ikura et al., 1992a), the differential spectra (CD of the complex subtracted from that of Ca^{2+}-CaM) indicates the secondary structure of

Orai-CMBD in the complex (dashed line in Figure 15B). The peptide shows a partial helix formation with $\theta_{220}/\theta_{209}$ = 0.71 consistent with the crystal structure (Liu et al., 2012). The peptide alone displayed a $\theta_{220}/\theta_{209}$ of 0.46 (Figure 15A) suggesting that helical content is only induced when complexed. While significant secondary structure changed was observed upon Orai-CMBD binding for CaM, CaM(1TnC) and CaM(2TnC), minimal change was observed for CaM(3TnC) and CaM(4TnC) (Table 5). This is slightly surprising as our ITC, quenching and lifetime studies all indicated a similar binding mode for CaM, CaM(3TnC) and CaM(4TnC). To provide a better explanation, we next created theoretical three-dimensional models of the chimeras to assess the stereochemical environment of peptide binding.

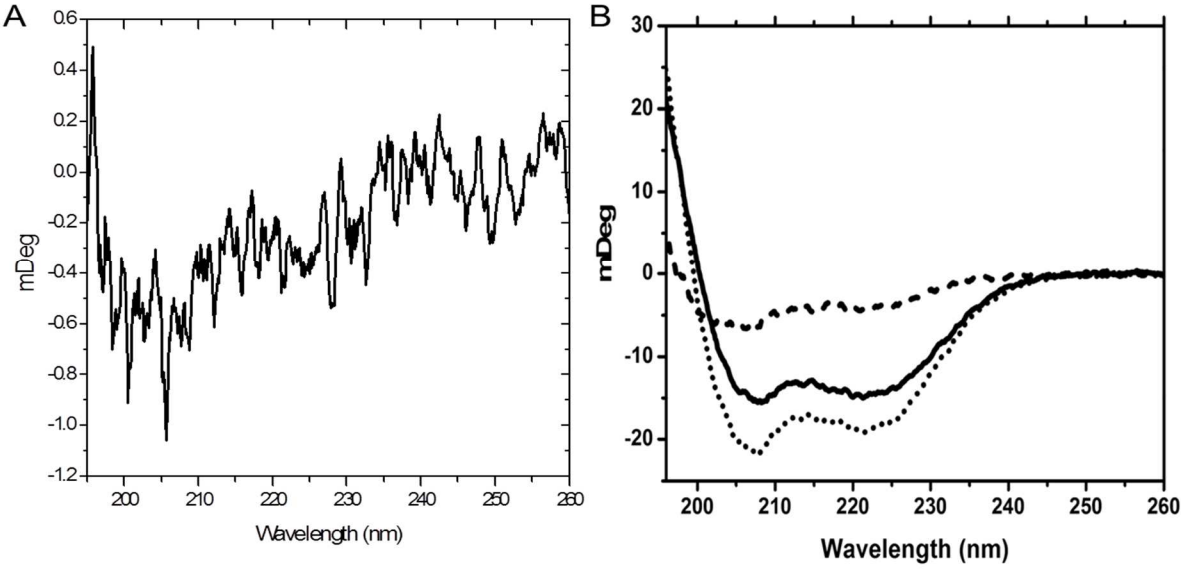

Figure 15: Circular Dichroism spectra of Orai-CMBD alone and complexed with CaM. (A) The CD spectra of the Orai-CMBD peptide alone, displaying unstructual characteristics. **(B)** The CD spectra of CaM were recorded in the presence of Ca^{2+} (solid line) and Ca^{2+} and Orai-CMBD (dotted line). Their differential spectrum (dashed line) presents the structure of Orai-CMBD in the complex assuming no CaM structural change upon ligand binding. Note that the CD unit was intentionally shown in degrees of light rotation because the CD spectra of CaM and the complexed Orai-CBMD have a very similar mean residual ellipticity.

Table 5: Ellipticity ratios for apo-, Ca^{2+}-, and Orai-CMBD-bound CaM and chimeras

	$\theta_{220}/\theta_{209}$ Apo	$\theta_{220}/\theta_{209}$ Ca^{2+}	$\theta_{220}/\theta_{209}$ Orai-CMBD
CaM	0.90 ± 0.02	0.991 ± 0.017	0.89 ± 0.02
CaM(1TnC)	0.884 ± 0.012	0.984 ± 0.012	0.926 ± 0.019
CaM(2TnC)	0.879 ± 0.004	0.989 ± 0.008	0.936 ± 0.019
CaM(3TnC)	0.902 ± 0.007	0.941 ± 0.009	0.947 ± 0.017
CaM(4TnC)	0.90 ± 0.02	0.92 ± 0.05	0.89 ± 0.06

3.7 Modeling and Solvent Accessible Calculations

To rationalize the experimental data on hydrophobic exposure upon Ca^{2+} binding, we modeled the chimera structures in the apo- and Ca^{2+}-bound forms by aligning the sequences of chimeras to the models of apo-CaM (PDB: 1CFC) and Ca^{2+}-CaM (PDB: 1CLL) as described in the experimental section, assuming that all chimera proteins adopt a similar structure to that of CaM. Modeling structures were then subjected to solvent accessible surface area (ASA) calculations for non-polar/apolar area (ASA_{ap}) and polar area (ASA_p) using 1.4 Å as the van der Waals (VDW) radius and a value of 5 for dot-density. The results of the calculations agree with conventional thinking in that the higher hydrophobic surface difference between apo and holo forms (i.e. ΔASA_{ap}) is expected as seen in CaM, in which the apolar surface increases 555 $Å^2$. However, a decrease of polar surface difference (ΔASA_p), including those negatively charged residues, of 693 $Å^2$ is also expected. Such surface changes are consistent with data from the ANS studies if one considers that ANS-sensitive proteins have to 1) induce more hydrophobic surface to interact with the aromatic portion of ANS, and 2) decrease the exposure of negatively charged residues so there becomes less repulsion between ANS sulfonate groups and the acidic protein. We then

performed a similar calculation using the modeled chimera structures, in which the chimera backbone was aligned with CaM while the orientations of the side chains were optimized. Based on the calculation, there was no strong correlation between the surface exposure and experimental data as depicted in that of CaM(1TnC) and CaM(2TnC) having a more positive ΔASA_{ap} (733 and 699 $Å^2$) and also a more negative ΔASA_p (−852 $Å^2$ and −861 $Å^2$). Nevertheless, the calculated ΔASA_{ap} areas (341 $Å^2$ and 486 $Å^2$) for CaM(3TnC) and CaM(4TnC) are consistent with the ANS binding from ITC and fluorescence studies, where the lower ANS fluorescence was observed. Note that the extra amino acids in CaM(1TnC) could not be modeled into the crystal structures and it was assumed that no conformational change upon Ca^{2+} binding occurred. Thus, the contribution of this extra sequence was canceled out in the ΔASA calculation. Similarly, the extra His-tagged sequence in 3TnC was treated in the same fashion.

Our experimental data suggests that chimera proteins such as CaM(1TnC) and CaM(2TnC) probably adopt a different structure than CaM in the N-terminal lobe. In fact, the structural alignment of CaM (PDB: 1CLL) and sTnC (4TnC) indicated that both structures cannot be aligned well given the root-mean square-deviation (RMSD) value of 6.8181 Å for all atoms. However, if a specific terminal lobe is aligned, the C-terminus gave RMSD = 0.856 Å while the N-terminus gave RMSD = 5.2 Å. Thus, it is unlikely that the N-terminal end of the chimera proteins, such as 1TnC and 2TnC, will adopt a similar structure as CaM.

The crystal structure of the CaM/Orai-CMBD complex is intriguing because the structure of Ca^{2+}-CaM is not perturbed after ligand binding. The structural alignment of CaM complexed with Orai-CMBD to Ca^{2+}-CaM reveals identical structures with RMSD =

0.459 Å. The experimental characterization in solution, including ours, all points to the complexation of two Orai-CMBD molecules that have similar binding affinities and occupy similar binding environments as judged from Trp76 fluorescence, but can still be differentiated by CaM(1TnC) and CaM(2TnC).

3.8 Rationale of Experimental Data with the Existing Structural Information of CaM/Orai-CMBD

The CaM/Orai-CMBD complex has been investigated by crystallography and NMR (Liu et al., 2012). The X-ray structure revealed that CaM adopts an unusual extended conformation with only one Orai-CMBD bound in the C-terminal lobe. However, NMR NOE indicated that CaM-N also interacts with Orai-CMBD, where both interactions for ligand binding are primarily hydrophobic. The reported ITC data also indicated a 1:2 stoichiometry of CaM/Orai-CMBD binding with the Orai-binding to CaM-C four times tighter (K_a = 9.1 x 10^5 M^{-1}) than CaM-N (K_a = 2.1 x 10^5 M^{-1}). Unambiguous evidence for the stoichiometry determination arose from the study of size exclusion chromatography, in which it showed that CaM is capable of binding two molecules of thioredoxin-fused Orai-CMBD. Therefore, the authors concluded that both the ligand binding sites of CaM-C and CaM-N are homologous. Our ITC data generally agreed with theirs and the fit ("one site of sets" model and N = ~2) indicates that both binding sites are very similar in terms of thermodynamics. With the exchanged EF1 and EF2, the ITC thermograms showed a very interesting binding, which could only be fit to a two-sequential binding sites model. The results revealed that the N-terminal lobe of CaM(1TnC) and CaM(2TnC) have a 40 times lower binding affinity and a

lower enthalpy change to Orai-CMBD than that of their C-terminal lobe. For a sequential binding, the ligand has to bind the higher affinity binding site before binding to the lower affinity site. The basis for this observation is not clear given that two lobes of CaM are considered to be functionally independent. Thus, our results possibly suggest that CaM(1TnC) and CaM(2TnC) form an unexpected structure, in which conformational change in domains may affect the central linker region that allows the signal to propagate from one lobe to the other. In TnC, the movement of helices that transmits the conformational change over substantial distances has been cited (Bayley et al., 1988) and thermodynamic evidence supports the cooperativity of both lobes (Skowronsky et al., 2013). This might be particularly applicable to CaM(2TnC) since there are additional residues located in its linker region that are believed to alter the binding structure. On the other hand, the exchanged EF3 and EF4 have less profound impact on the Orai-CMBD binding, displaying a similar binding mode to that of CaM.

In the complex, Orai-CMBD adopts a partial helical structure in the crystal structure, which is confirmed in solution by our CD measurements. The Trp76 residue of Orai-CMBD is deeply buried in a hydrophobic patch formed by several hydrophobic residues in CaM-N and CaM-C (Figure 16). The peptide binds to a tunnel formed with a low-charged surface (gray color in the electrostatic potential map). The negatively-charged surface of CaM is primarily located near both ends of the peptide.

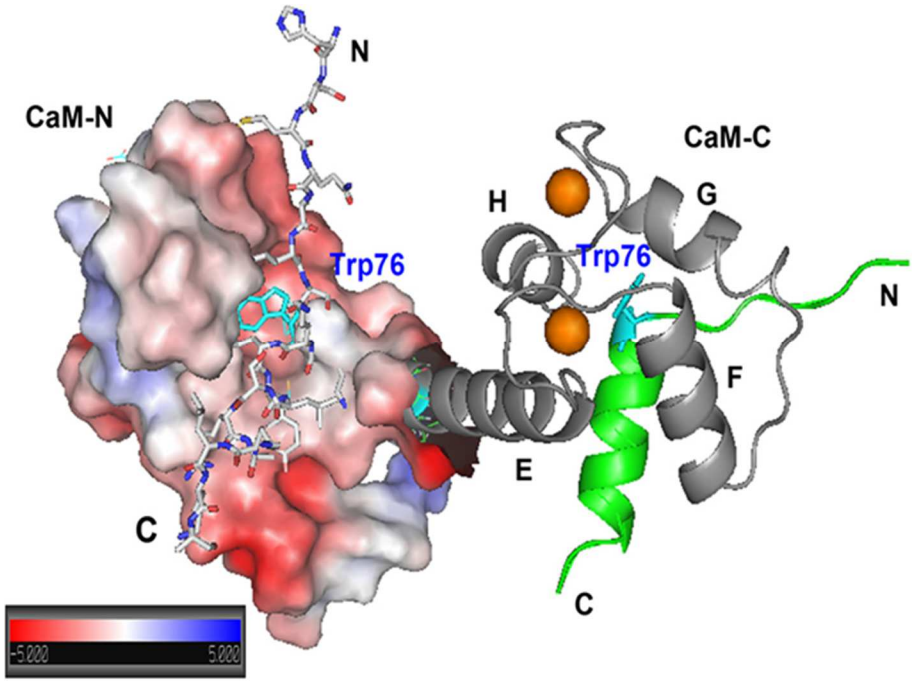

Figure 16: The proposed model of the 1:2 CaM/Orai-CMBD complex. The coordinates for the proposed model were obtained as a courtesy from Dr. Birnbaumer (NIH). One of two peptides (stick model) forms a partial helix structure and is bound in the hydrophobic patch (primarily gray) formed by CaM-N, shown as an electrostatic potential surface, where Trp76 (cyano) is deeply buried. The other Orai-CMBD shown in cartoon model (green) is flanked by the Ca^{2+}-bound (orange) EF-hands in CaM-C.

Based on the crystal and NMR study, CaM/Orai-CMBD binding appears to be dominated by hydrophobic interactions from Leu73, Trp76, and Leu79 from Orai-CMBD with the hydrophobic residues provided from CaM. The electrostatic interaction formed by residues, such as Lys and Arg in the CMBD and Glu in CaM, as seen in other CaM/CMBD systems (Clore et al., 1993), is essentially not significant in this system. Those hydrophobic residues for the interaction in CaM are similar in the chimeras except for I63V (numbering in CaM) in CaM(2TnC) and M124I, I125M, V136I, and M144F in CaM(4TnC) (Figure 17A). The substitution of Met to Ile, or vice versa, has been shown to have very minor effects on protein structure (Ratnaparkhi and Varadarajan, 2000; Lipscomb et al., 1998; Ohmura et al., 2001). Similarly, other residue substitutions, such as Val and Phe, should retain the

hydrophobic interaction with the ligand, given that the side chains of CaM are usually dynamic in solution (Lee et al., 2000). Thus, it appears that the C-terminal lobes of the chimeras are flexible enough to adopt a structure similar to CaM to facilitate CMBD binding, as suggested by ANS lifetime fluorescence. On the other hand, the N-terminal lobes of the chimeras apparently have a different structure compared to that of CaM (even with only one residue change in the CMBD binding site of CaM(2TnC)) and/or are not flexible enough for packing their side chains for ligand binding, given the lower enthalpy and higher solvent accessible quenching as seen in ITC and quenching studies. Such results provide an explanation for the 40 times lower binding affinity than that of C-terminal lobe. Another key residue for the complex formation, Leu79, is also embedded into a hydrophobic surface in CaM-C, whereas CaM(3TnC) has additional residues substituted, such as V108M, M109L, and I112T (Figure 17B). The substitution of Ile by the polar residue Thr appears to have no major impact for ligand binding. However, the hypothetical model of CaM-N did not have optimal side chain packing for Leu79 and reorganization of its side chains is essential for binding. Nevertheless, the hydrophobic patches for interacting with Trp76 and Leu79 remain similar for CaM(3TnC) and CaM(4TnC), resulting in a compatible binding affinity. Apparently, the N-terminal lobe of CaM(1TnC) and CaM(2TnC) cannot be explained purely by residue substitution as depicted in modeling studies, suggesting they might adopt a dissimilar structure to that of CaM. The change in structure is most likely observed on the three dimensional level, rather than that of secondary structure given that CaM and chimeras have relatively similar extents of secondary structure in the apo and Ca^{2+} bound forms as demonstrated by CD.

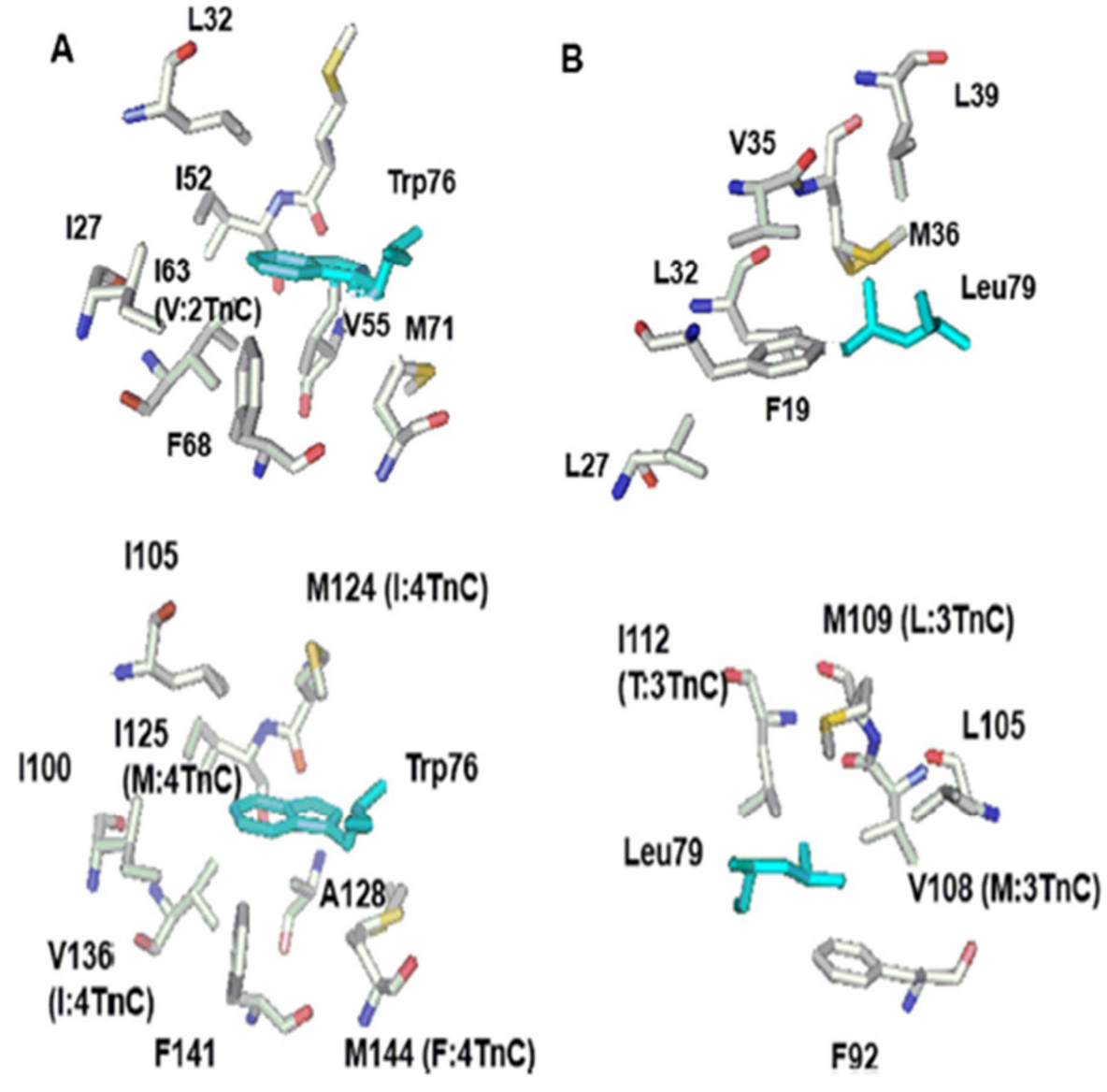

Figure 17: The hypothetical interaction of Orai-CMBD to CaM-N and CaM-C. The residues of Leu73, Trp76, and Leu79 are major contributors to the binding of CaM. In the Trp76 vicinity, the residues in one letter abbreviation in CaM-C are from the crystal structure while those in CaM-N are a hypothetical prediction **(A)**. The alteration in the position and chimeras are shown in parentheses. Leu79 is located in the forming helix and interacts with hydrophobic residues **(B)**. Note that the numbering of residues is one residue off from Figure 1 since the first Met residue is not included in the crystal structure. We used the same numbering convention as the reference in this figure and within the text for clarity.

CHAPTER 4

CONCLUSIONS

Here we used the fluorescent dye ANS to probe the structures of CaM and chimera proteins in the absence and presence of Ca^{2+}. ANS studies revealed that the exchanged EF-hands alter ANS fluorescence intensity. However, such an intensity measurement, which is typically interpreted as "hydrophobicity", should be carefully explained with the assistance of lifetime and binding affinity studies as described in this report. Here, we are the first to show that steady-state ANS enhancements do not always correlate with binding affinity, debunking a common assumption. Such results will clearly have a profound impact, as ANS fluorescent studies are frequently employed to monitor protein unfolding and conformational changes. Lifetime measurements indicated ANS heterogeneity, in which two different ANS environments with distinct fluorescence dynamic decays were observed. Such ANS heterogeneity is most likely attributed to the two excited levels, which are altered by the exchanged EF-hands, especially EF1 and EF2. Among the chimeras, CaM(3TnC) appears to have a lower ANS binding affinity. Such a low induced hydrophobicity change might suggest an inability for CMBD binding. However, thermodynamics of CaM/Orai-CMBD revealed a surprisingly poor correlation between ANS fluorescence and ligand binding, given that CaM(3TnC) still retains a similar binding affinity as that of CaM. Thus, our data strongly suggests that the induced hydrophobic surface assessed from ANS binding does not participate in the binding to Orai-CMBD. Rather, the determined hydrophobicity most likely reflects the interactions essential for enzyme activation, separate from CMBD binding. In fact, this conclusion agrees with the fact that Ca^{2+}-CaM(3TnC) is not retained on hydrophobic interaction chromatography (HIC), unlike CaM and the other chimeras.

We also used CaM and chimera proteins to investigate the interaction with Orai-CMBD and rationalized our data assisted by a published crystal structure. Structural studies by *Liu et al.* (2012) proposed a unique CaM binding mode, in which two target Orai peptides are bound to one CaM protein, where minimal conformational change is observed upon ligand binding, resembling the open, Ca^{2+}-bound CaM structure. Open CaM conformations bound to target peptides have been historically hard to crystallize given their significant structural heterogeneity (Nagulapalli et al., 2012). Additionally, studies evaluating the CaM/calcineurin A complex have indicated disparity between the crystallographic structure and solution structure binding stoichiometry and conformation. The crystal structure of the complex was reported to be in an open, extended conformation, in which two peptides are surrounded by two CaM proteins (Ye et al., 2006; Ye et al., 2008), whereas the solution structure mirrored a 1:1 collapsed binding mode (Majava and Kursula, 2009). Thus, while CaM-peptide complexes may provide accurate details on protein-level interactions, given that the CaM-regulatory regions are often very flexible, the crystals may be biologically non-relevant as the conformation could be driven by the crystallization process (Kursula, 2014a). Additionally, the central helix linker in CaM tends to bend and unfold in the absence of a ligand (Baber et al., 2001) and as a result is poorly defined in crystal structures (Kursula, 2014b). Taken together, such results bring into question the value of the crystal structure and the proposed stoichiometry.

In evaluation of our experimental data, strictly speaking, the complex can also be explained by a canonical CaM/CMBD model given that only a single Orai-CMBD signal was detected in quenching and kinetic studies. However, the ITC data of chimeras clearly differentiates the two binding sites, thus a single peptide binding mode observed in some of

our studies may be due to the homologous structures of CaM-C and CaM-N, such that average values were obtained. The observed binding constant for the CaM/Orai-CMBD complex is physiologically weak/moderate, being on the order of 10^5 M^{-1}. Given the multi-subunit orientation of the STIM1/Orai1 CRAC channel, for CaM to bind to two separate Orai1 N-terminal domains is not only plausible, but may be a necessity for CDI initiation given the weak binding. To gain additional insights on how CaM promotes CDI in relation to both STIM1 and Orai1, our future work will entail developing a FRET-based assay where STIM1 and wt/E106D Orai1are extrinsically labeled. Previous studies have used FRET extensively to monitor the conformational changes elicited upon STIM1 CAD binding to Orai1 (Navarro-Borelly et al., 2008; Calloway et al., 2010; Fahrner et al., 2014). By exposing CaM to the STIM1/Orai1 complex, a decrease in FRET would indicate that CaM promotes STIM1 dissociation to inactivate the channel as previously proposed (Liu et al., 2012). Additionally, by using E106D Orail, we can investigate if such a mutation allosterically modulates the CaM binding domain of Orai1 when in complex with STIM1, as proposed previously as a possible regulatory function of CDI (Scrimgeour et al., 2014). Coupled together with the physical data presented here, these FRET based assays will provide a well-rounded depiction of the molecular mechanism for CDI.

In addition to providing knowledge on the CaM/Orai1 interaction, our data also set forth informative details about the chimera proteins. Contrary to previous assumptions, our experimental data indicates that the structural models for CaM(1TnC) and CaM(2TnC) are not reliable, especially in their N-terminal lobe, suggesting that structurally the chimeras may differ from the CaM template. Additionally, it is unclear whether or not the exchanged EF-hands should have a similar impact on all CaM/CMBD systems because CaM in the

CaM/Orai-CMBD complex adopts an unusual extended structure, interacting with the ligand primarily through hydrophobic forces. Our preliminary data from a collapsed 1:1 CaM/CaMKII model indicated a different observation in response to ANS (unpublished results). Its ANS fluorescence dropped 1.5 fold and shifted λ_{max} from 480 to 450 nm upon the complex formation. This decrease was not due to the change in ANS binding affinity, but rather the shorter lifetime component being significantly smaller compared with CaM/Orai-CMBD. Furthermore, one may also anticipate that the exchanged EF1 and EF2 will result in a similar impact on other CMBD binding. Our preliminary data using the CMBD of the Fas associated death domain (FADD) has shown in some cases the exchanged EF3 and EF4, not EF1 and EF2, impair the ligand binding (unpublished results). The study here addressed the first attempt to investigate the relationship of ANS-probed hydrophobicity and its interaction with a CMBD peptide via spectroscopy, thermodynamic and kinetic approaches. Thus, extensions from this study to other known CaM/CMBD systems and to studies using whole target enzymes will help understand the divergence of structure and function of CaM.

REFERENCES

Baber, J. L.; Szabo, A.; Tjandra, N. Analysis of slow interdomain motion of macromolecules using NMR relaxation data. *J Am Chem Soc*. **2001**, *123*, 3953-3959.

Babu, Y. S.; Sack, J. S.; Greenhough, T.J.; Bugg, C. E.; Means, A. R.; Cook, W. J. Three-dimensional structure of calmodulin. *Nature.* **1985**, *315*(6014): 37-40.

Babu, Y. S.; Bugg, C. E.; Cook, W. J. Structure of calmodulin refined at 2.2 A resolution. *J Mol Biol.* **1988**, *204*(1):191–204.

Babich, O.; Matveev, V.; Harris, A. L.; Shirokov, R. Ca^{2+}-dependent inactivation of $Ca_V1.2$ channels prevents Gd^{3+} block: does Ca^{2+} block the pore of inactivated channels? *J. Gen. Physiol.* **2007**, *129*, 477-483.

Bayley, P.; Martin, S.; Jones, G. The conformation of calmodulin: a substantial environmentally sensitive helical transition in Ca4-calmodulin with potential mechanistic function. *FEBS Lett.* **1988**, *238*(1):61-6.

Bayley, P. M.; Findlay, W. A.; Martin, S. R. Target recognition by calmodulin: dissecting the kinetics and affinity of interaction using short peptide sequences. *Protein Sci.* **1996**, *5*(7):1215-28.

Berridge, M. J.; Bootman, M. D.; Roderick, H. L. Calcium signaling: Dynamics, homeostasis and remodeling. *Nat Rev Mol Cell Biol.* **2003**, *4*, 517–529.

Berridge, M. J. Ion Channels. *Cell Signaling Biology.* **2012**, 3.1-3.71.

Bers, D. M. Cardiac excitation-contraction coupling. *Nature.* **2002**, *415*, 198–205.

Biasini, M.; Bienert, S.; Waterhouse, A.; Arnold, K.; Studer, G.; Schmidt, T.; et al. SWISS-MODEL: modelling protein tertiary and quaternary structure using evolutionary information. *Nucleic Acids Res.* **2014**, *42* (Web Server issue):W252–8.

Bootman, M. D. Calcium signaling. *Cold Spring Harb Perspect Biol*. **2012**, *4*, (7): a011171.

Bordoli, L.; Kiefer, F.; Arnold, K.; Benkert, P.; Battey, J.; Schwede, T. Protein structure homology modeling using SWISS-MODEL workspace. *Nat Protoc.* **2009**, *4*(1):1-13.

Brown, M. S.; Goldstein, J. L. A proteolytic pathway that controls the cholesterol content of membranes, cells and blood. *PNAS.***1999**, *96*, 11041–11048.

Calloway, N.; Holowka, D.; Baird, B. A Basic Sequence in STIM1 Promotes Ca^{2+} Influx by Interacting with the C-Terminal Acidic Coiled Coil of Orai1. *Biochemistry*. **2010**, *49*, 1067-1071.

Cheng, X.; Patterson, T. A. Construction and use of X PL promoter vectors for direct cloning and high level expression of PCR amplified DNA coding sequences. *Nucleic Acids Research*. **1992**, *20*,(17):4591-4598.

Clapham, D. E. A STIMulus package puts Orai calcium channels to work. *Cell*. **2009**, *136*.

Clore, G. M.; Bax, A.; Ikura, M.; Gronenborn, A. M. Structure of calmodulin-target peptide complexes. *Curr Opin Struct Biol.* **1993**, *3*(6): 838–45.

D'Alfonso, L.; Collini, M.; Baldini, G. Evidence of heterogeneous 1-anilinonaphthalene-8-sulfonate binding to beta-lactoglobulin from fluorescence spectroscopy. *Biochim Biophys Acta*. **1999**, *1432*(2):194–202.

Derler, I.; Fahrner, M.; Carugo, O.; Muik, M.; Bergsmann, J.; Schindl, R.; Frischauf, I.; Eshaghi, S.; Romanin, C. Increased hydrophobicity at the N-terminus/membrane interface impairs gating of the SCID related ORAI1 mutant. *J Biol Chem*. **2009**, *284*, 15903–15915.

Dolinsky, T. J.; Nielsen, J. E.; McCammon, J. A.; Baker, N. A. PDB2PQR: an automated pipeline for the setup of Poisson-Boltzmann electrostatics calculations. *Nucleic Acids Res.* **2004**, *32*(Web Server issue):W665–7.

Dupont, G.; Combettes, L.; Bird, G. S.; Putney, J. W. Calcium oscillations. *Cold Spring Harb Perspect Biol*. **2011**, *3*: a004226.

Fahrner, M.; Muik, M.; Schindl, R.; Butorac, C.; Stathopulos, P.; Zheng, L.; Jardin, I.; Ikura, M.; Romanin C. A coiled-coil clamp controls both conformation and clustering of stromal interaction molecule 1 (STIM1). *J Biol Chem*. **2014**, *289*(48): 33231-33244.

Ferri, K. F.; Kroemer, G. Organelle-specific initiation of cell death pathways. *Nature Cell Biol.* **2001**, *3*, E255–E263.

Feske, S.; Muller, J. M.; Graf, D.; Kroczek, R. A.; Drager, R.; Niemeyer, C.; Baeuerle, P. A.; Peter, H. H.; Schlesier, M. Severe combined immunodeficiency due to defective binding of the nuclear factor of activated T cells in T lymphocytes of two male siblings. *Eur J Immunol*. **1996**, *26*, 2119–26.

Feske, S.; Prakriya, M.; Rao, A.; Lewis, R.S. A severe defect in CRAC Ca^{2+} channel activation and altered K^+ channel gating in T cells from immunodeficient patients. *J. Exp. Med.* **2005**, *202*, 651-662.

Feske, S.; Gwack, Y.; Prakriya, M.; Srikanth, S.; Puppel, S. H.; Tanasa, B.; et al. A mutation in Orai1 causes immune deficiency by abrogating CRAC channel function. *Nature.* **2006**, *441*, 179-85.

Fidalgo Da Silva, E.; Freire, M. M.; Barrabin, H.; Sorenson, M. M.; Tikunova, S.; Johnson, J. D.; et al. Troponin C/calmodulin chimeras as erythrocyte plasma membrane Ca^{2+}-ATPase activators. *Int J Biochem Cell Biol*. **2006**, *38*(2):209-21.

Fraczkiewicz, R.; Braun, W. Exact and Efficient Analytical Calculation of the Accessible Surface Areas and Their Gradients for Macromolecules. *J Comp Chem*. **1998**, *19*:319-33.

Frischauf, I.; Muik, M.; Derler, I.; Bergsmann, J.; Fahrner, M.; Schindl, R.; Groschner, K.; Romanin, C. Molecular determinants of the coupling between STIM1 and Orai channels: differential activation of Orai1-3 channels by a STIM1 coiled-coil mutant. *J. Biol. Chem.* **2009**, *284*, 21696-21706.

Gachhui, R.; Abu-Soud, H. M.; Ghosha, D. K.; Presta, A.; Blazing, M. A.; Mayer, B.; et al. Neuronal nitric-oxide synthase interaction with calmodulin-troponin C chimeras. *J Biol Chem*. **1998**, *273*(10):5451-4.

Galione, A. NAADP receptors. *Cold Spring Harb Perspect Biol*. **2011**, *3*: a004036.

George, S. E.; VanBerkum, M. F. A.; Ono, T.; Cook, R.; Hanle, R. M.; Putkey, J. A.; Means, A. R. Chimeric Calmodulin-Cardiac Troponin C Proteins Differentially Activate Calmodulin Target Enzymes. *J Biol Chem*. **1990**, *265*(16): 9228-9235.

George, S. E.; Su, Z.; Fan, D.; Means, A. R. Calmodulin-cardiac troponin C chimeras. Effects of domain exchange on calcium binding and enzyme activation. *J Biol Chem.* **1993**, *268*(33):25213-20.

George, S. E.; Su, Z.; Fan, D.; Wang, S.; Johnson, J. D. The Fourth EF-Hand of Calmodulin and Its Helix-Loop-Helix Components: Impact on Calcium Binding and Enzyme Activation. *Biochemistry.* **1996,** *35,* 8307-8313.

Gifford, J. L.; Walsh, M. P.; Vogel, H. J. Structures and metal ion- binding properties of the Ca^{2+}-binding helix-loop-helix EF-hand motifs. *Biochem. J.* **2007**, *405*, 199–221.

Gorelick, F. S.; Shugrue, C. Exiting the endoplasmic reticulum. *Mol Cell Endocrinol.* **2001**, *177*, 13-18.

Guex, N.; Peitsch, M. C. SWISS-MODEL and the Swiss-PdbViewer: an environment for comparative protein modeling. *Electrophoresis.* **1997**, *18*(15):2714-23.

Hewavitharana, T. D. X.; et.al. Role of STIM and Orai proteins in the store-operated calcium signaling pathway. *Cell Calcium.* **2007**, *42*, 173-182.

Holowka, D.; Calloway, N.; Cohen, R.; Gadi, D.; Lee, J.; Smith, N. L.; Baird, B. Roles for Ca^{2+} mobilization and its regulation in mast cell functions. *Frontiers in Immunology*. ***2012***, 3, *104.*

Hoover, P. J.; Lewis, R. S. Stoichiometric requirements for trapping and gating of Ca^{2+} release-activated Ca^{2+} (CRAC) channels by stromal interaction molecule 1 (STIM1). *PNAS*. **2011**, *108*, 13299-13304.

Hou, X.; Pedi, L.; Diver, M. M.; Long, S. B. Crystal structure of the calcium release activated calcium channel Orai. *Science*. **2012**, 338,1308-1313.

Ikura, M.; Clore, G. M.; Gronenborn, A. M.; Zhu, G.; Klee, C. B.; Bax, A. Solution structure of a calmodulin-target peptide complex by multidimensional NMR. *Science.* **1992a**, *256*(5057):632-8.

Ikura, M.; Barbato, G.; Klee, C. B.; Bax, A. Solution structure of calmodulin and its complex with a myosin light chain kinase fragment. *Cell Calcium.* **1992b**, *13*(6–7):391-400.

Jha, A.; Ahuja, M.; Maleth, J.; Moreno, C. M.; Yuan, J. P.; Kim, M. S.; Muallem, S. The STIM1 CTID domain determines access of SARAF to SOAR to regulate Orai1 channel function. *J Cell Biol*. **2013**, *202*, 1.

Ji, W.; Xu, P.; Li, Z.; Lu, J.; Liu, L.; Zhan, Y.; Chen, Y.; Hille, B.; Xu, T.; Chen, L. Functional stoichiometry of the unitary calcium-release-activated calcium channel. *PNAS.* **2008**, *105*,13668-13673.

Kaufman, R. J. Stress signaling from the lumen of the endoplasmic reticulum: coordination of gene transcriptional and translational controls. *Genes Dev.* **1999**, *13*, 1211–1233.

Kilch, T.; Alansary, D.; Peglow, M.; Dorr, K.; Rychkov, G.; Rieger, H.; Peinelt, C.; Niemeyer, B. A. Mutations of the Ca^{2+}-sensing stromal interaction molecule STIM1 regulate Ca^{2+} influx by altered oligomerization of STIM1 and by destabilization of the Ca^{2+} channel Orai1. *J. Biol. Chem.* **2013**, *288*, 1653-1664.

Kincaid, R. L.; Vaughan, M.; Osborne, J. C.; Tkachuk, V. A. Ca^{2+}-dependent interaction of 5-dimethylaminonaphthalene-1-sulfonyl-calmodulin with cyclic nucleotide phosphodiesterase, calcineurin, and troponin I. *J Biol Chem.* **1982**, *257*(18):10638-43.

Kleerekoper, Q. K.; Putkey, J. A. PEP-19, an intrinsically disordered regulator of calmodulin signaling. *J Biol Chem.* **2009**, *284*(12):7455-64.

Kretsinger, R. H.; Rudnick, S. E.; Weissman, L. J. Crystal structure of calmodulin. *J Inorg Biochem.* **1986**, *28*(2–3):289-302.

Kursula, P. The many structural faces of calmodulin: a multitasking molecular jackknife. *Amino Acids.* **2014a**, *46*(10): 2295-304.

Kursula, P. Crystallographic snapshots of initial steps in the collapse of calmodulin central helix. *Acta Crystallogr D Biol Crystallogr.* **2014b**, *70*, 24-30.

Lee, A. L.; Kinnear, S. A.; Wand, A. J. Redistribution and loss of side chain entropy upon formation of a calmodulin-peptide complex. *Nat Struct Biol*. **2000**, *7*(1):72-7.

Lee, K. P.; Yuan, J. P.; Zeng, W.; So, I.; Worley, P. F.; Muallem, S. Molecular determinants of fast Ca^{2+}-dependent inactivation and gating of the Orai channels. *PNAS.* **2009**, *106*, 14687-14692.

Levitan, I. B. It is calmodulin after all! Mediator of the calcium modulation of multiple ion channels. *Neuron* **1999**, *22*, 645-648.

Lewit-Bentley, A.; Re´ty, S. EF-hand calcium-binding proteins. *Curr. Opin. Struct. Biol.* **2000**, *10*, 637-643.

Li, Z.; Liu, L.; Deng, Y.; Ji, W.; Du, W.; Xu, P.; Chen, L.; Xu, T. Graded activation of CRAC channel by binding of different numbers of STIM1 to Orai1 subunits. *Cell Res.* **2011**, *21*, 305-315.

Lipscomb, L. A.; Gassner, N. C.; Snow, S. D.; Eldridge, A. M.; Baase, W. A.; Drew, D. L.; et al. Context-dependent protein stabilization by methionine-to-leucine substitution shown in T4 lysozyme. *Protein Sci.* **1998**, *7*(3):765–73.

Liou, J.; Kim, M. L.; Heo, W. D.; Jones, J. T.; Myers, J. W.; Ferrell, J. E. STIM is a Ca^{2+} sensor essential for Ca^{2+}-store-depletion-triggered Ca^{2+} influx. *Curr Biol.* **2005**, *15*, 1235-41.

Liu, Y.; Zheng, X.; Mueller, G. A.; Sobhany, M.; DeRose, E. F.; Zhang, Y.; et al. Crystal structure of calmodulin binding domain of orai1 in complex with Ca^{2+} calmodulin displays a unique binding mode. *J Biol Chem.* **2012**, *287*(51):43030-41.

Locke, E. G.; Bonilla, L.; Liang, Y.; Takita, Y.; Cunningham, K. W. A homolog of voltage-gated Ca^{2+} channels stimulated by depletion of secretory Ca^{2+} in yeast. *Mol Cell Biol.* **2000**, *20*, 6686–6694.

Macian, F. NFAT proteins: key regulators of T-cell development and function. *Nat. Rev. Immunol.* **2005**, *5* (6): 472–84.

Majava, V.; Kursula, P. Domain swapping and different oligomeric states for the complex between calmodulin and the calmodulin-binding domain of calcineurin A. *PLoS One*. **2009**, *4*, e5402.

Manji, S. S.; Parker, N. J.; Williams, R. T.; van Stekelenburg, L.; Pearson, R. B.; Dziadek, M.; Smith, P. J. STIM1: a novel phosphoprotein located at the cell surface. *Biochim. Biophys. Acta*. **2000**, *1481*,147–155.

Martin, S. R.; Bayley, P. M. The effects of Ca^{2+} and Cd^{2+} on the secondary and tertiary structure of bovine testis calmodulin. A circular-dichroism study. *Biochem J.* **1986**, *238*(2):485-90.

Matsubara, M.; Hayashi, N.; Titani, K.; Taniguchi, H. Circular dichroism and 1H NMR studies on the structures of peptides derived from the calmodulin-binding domains of inducible and endothelial nitric-oxide synthase in solution and in complex with calmodulin. Nascent alpha-helical structures are stabilized by calmodulin both in the presence and absence of Ca^{2+}. *J Biol Chem.* **1997**, *272*(37):23050–6.

Meador, W. E.; Means, A. R.; Quiocho, F. A. Target enzyme recognition by calmodulin: 2.4 A structure of a calmodulin-peptide complex. *Science.* **1992**, *257*(5074):1251-5.

Miao, Y.; Miner, C.; Zhang, L.; Hanson, P. I.; Dani, A.; Vig, M. An essential and NSF independent role for α-SNAP in store-operated calcium entry. *eLife*. **2013**, *2*.

Moorthy, A. K.; Gopal, B.; Satish, P. R.; Bhattacharya, S.; Bhattacharya, A.; Murthy, M. R.; et al. Thermodynamics of target peptide recognition by calmodulin and a calmodulin analogue: implications for the role of the central linker. *FEBS Lett.* **1999**, *461*(1–2):19-24.

Mullins, F. M.; Park, C. Y.; Dolmetsch, R. E.; Lewls, R. S. STIM1 and calmodulin interact with orai1 to induce Ca^{2+} dependent inactivation of CRAC channels. *PNAS*. **2009**, *106* (36), 15495-15500.

Nagulapalli, M.; Parigi, G.; Yuan, J.; Gsponer, J.; Deraos, G.; Bamm, V. V.; Harauz, G.; Matsoukas, J.; de Planque, M. R.; Gerothanassis, T. P.; Babu, M. M.; Luchinat, C.; Tzakos, A. G. Recognition pliability is coupled to structural heterogeneity: a calmodulin intrinsically disordered binding region complex. *Stucutre*. **2012**, *20*, 522-533.

Nalefski, E. A.; Falke, J. J. Cation charge and size selectivity of the C2 domain of cytosolic phospholipase A2. *Biochemistry.* **2002**, *41*, 1109-1122.

Navarro-Borelly, L.; Somasundaram, A.; Yamashita, M.; Ren, D.; Miller, R. J.; Prakriya, M. STIM1-Orai1 interactions and Orai1 conformational changes revealed by live-cell FRET microscopy. *J Physiol.* **2008**, *586*, 5383–401.

Newman, E.; Spratt, D. E.; Mosher, J.; Cheyne, B.; Montgomery, H. J.; Wilson, D. L.; et al. Differential activation of nitric-oxide synthase isozymes by calmodulin-troponin C chimeras. *J Biol Chem.* **2004**, *279*(32):33547-57.

Ohmura, T.; Ueda, T.; Hashimoto, Y.; Imoto, T. Tolerance of point substitution of methionine for isoleucine in hen egg white lysozyme. *Protein Eng.* **2001**, *14*(6): 421-5.

O'Neil, K. T.; DeGrado, W. F. How calmodulin binds its targets: Sequence independent recognition of amphiphilic α-helices. *Trends Biochem Sci.* **1990**, *15*, 59-64.

Palty, R.; Raveh, A.; Kaminsky, I.; Meller, R.; Reuveny, E. SARAF Inactivates the Store Operated Calcium Entry Machinery to Prevent Excess Calcium Refilling. *Cell*. **2012**, *149*, 425-438.

Parekh, A.; Putney, J. W. Store Operated Calcium Channels. *Physiological Reviews.* **2005**, *85*, 757-810.

Park, C. Y.; Hoover, P. J.; Mullins, F. M.; Bachhawat, P.; Covington, E. D.; Raunser, S.; et al. STIM1 clusters and activates CRAC channels via direct binding of a cytosolic domain to Orai1. *Cell.* **2009**, *136*, (5):876-90.

Partiseti, M.; Ledeist, F.; Hivroz, C.; Fischer, A.; Korn, H.; Choquet, D. The calcium current activated by T cell receptor and store depletion in human lymphocytes is absent in a primary immunodeficiency. *J Biol Chem.* **1994**, *269*, 32327–32335.

Picard, C.; McCarl, C. A.; Papolos, A.; Khalil, S.; Luthy, K.; Hivroz, C.; LeDeist, F.; Rieux-Laucat, F.; Rechavi, G.; Rao, A.; Fischer, A.; Feske, S. STIM1 mutation associated with a syndrome of immunodeficiency and autoimmunity. *N Engl J Med*. **2009**, *360*, 1971–80.

Pidcock, E.; Moore, G. R. Structural characteristics of protein binding sites for calcium and lanthanide ions. *J. Biol. Inorg. Chem.* **2001**, *6*, 479-489.

Prakriya, M.; Feske, S.; Gwack, Y.; Srikanth, S.; Rao, A.; Hogan, P. G. Orai1 is an essential pore subunit of the CRAC channel. *Nature*. **2006**, *443*, 230-233.

Ratnaparkhi, G. S.; Varadarajan, R. Thermodynamic and structural studies of cavity formation in proteins suggest that loss of packing interactions rather than the hydrophobic effect dominates the observed energetics. *Biochemistry.* **2000**, *39*(40):12365-74.

Robinson, G. W.; Robbins, R. J.; Fleming, G. R.; Morris, J. M.; Knight, A. E. W.; Morrison, R. J. S. Picosecond studies of the fluorescence probe molecule 8-anilino-1-naphthalenesulfonic acid. *J Am Chem Soc.* **1978**, *100*:7145–50.

Saimi, Y.; Kung, C. Calmodulin as an ion channel subunit. *Annu Rev Physiol.* **2002**, *64*, 289-311.

Sali, A.; Blundell, T. L. Comparative protein modelling by satisfaction of spatial restraints. *J Mol Biol.* **1993**, *234*(3):779–815.

Scrimgeour, N.; Litjens, T.; Ma, L.; Barritt, G. J.; Rychkov, G. Y. Properties of Orai1 mediated store-operated current depend on the expression levels of STIM1 and Orai1 proteins. *J. Physiol.* **2009**, *587*, 2903-2918.

Scrimgeour, N. R.; Wilson, D. P.; Rychkov, G. Y. Glutamate 106 in the Orai1 pore contributes to fast Ca^{2+}-dependent inactivation and pH dependence of Ca^{2+} release-activated Ca^{2+} (CRAC) current. *Biochem. J.* **2012**, *441*, 743–753.

Scrimgeour, N. R.; Wilson, D. P.; Barritt, G. J.; Rychkov, G. Y. Structural and stoichiometric determinants of Ca^{2+} release-activated Ca^{2+} (CRAC) channel Ca^{2+}-dependent inactivation. *Biochim Biophys Acta.* **2014**, *1838*, 1281-1287.

Shixing, Y.; Haug, A. Ligand-triggered conformational perturbations elicit changes at the single cysteinyl residue of spinach calmodulin *Eur. J. Biochem.* **1988,** *175*, 119-124.

Singh, B. B.; Liu, X.; Tang, J.; Zhu, M. X.; Ambudkar, I. S. Calmodulin regulates Ca^{2+}-dependent feedback inhibition of store-operated Ca^{2+} influx by interaction with a site in the C terminus of TrpC1. *Mol Cell.* **2002**, *9*, 739–750.

Skowronsky, R. A.; Schroeter, M.; Baxley, T.; Li, Y.; Chalovich, J. M.; Spuches, A. M. Thermodynamics and molecular dynamics simulations of calcium binding to the regulatory site of human cardiac troponin C: evidence for communication with the structural calcium binding sites. *J Biol Inorg Chem*. **2013**, *18*(1):49-58.

Someya, Y.; Yui, H. Fluorescence lifetime probe for solvent microviscosity utilizing anilinonaphthalene sulfonate. *Anal Chem*. **2010**, *82*(13):5470-6.

Srikanth, S.; Jung, H. J.; Ribalet, B.; Gwack, Y. The intracellular loop of Orai1 plays a central role in fast inactivation of Ca^{2+} release-activated Ca^{2+} channels. *J. Biol. Chem.* **2009**, *285*, 5066-5075.

Srikanth, S.; Jung, H. J.; Kim, K. D.; Souda, P.; Whitelegge, J.; Gwack, Y. A novel EF-hand protein, CRACR2A, is a cytosolic Ca^{2+} sensor that stabilizes CRAC channels in T cells. *Nat. Cell Biol.* **2010**, *12*, 436-446.

Srivastava, A. K.; Sharma, Y.; Chary, K. V. A natively unfolded βγ-crystallin domain from *Hahella chejuensis*. *Biochemistry.* **2010**, *49*, 9746-9755.

Strynadka, N. C.; James, M. N. Model for the interaction of amphiphilic helices with troponin C and calmodulin. *Proteins.* **1990**, *7*(3):234-48.

Su, A. I.; Wiltshire, T.; Batalov, S.; Lapp, H.; Ching, K.A.; Block, D.; Zhang, J.; Soden, R.; Hayakawa, M.; Kreiman, G.; et al. A gene atlas of the mouse and human protein-encoding transcriptomes. *PNAS*. **2004**, *101*, 6062-6067.

Su, Z.; Blazing, M. A.; Fan, D.; George, S. E. The calmodulin-nitric oxide synthase interaction. Critical role of the calmodulin latch domain in enzyme activation. *J Biol Chem.* **1995**, *270*(49):29117-22.

Suko, J.; Pidlich, J.; Bertel, O. Calcium release from intact calmodulin and calmodulin fragment 78–148 measured by stopped-flow fluorescence with 2-p-toluidinylnaphthalene sulfonate. Effect of calmodulin fragments on cardiac sarcoplasmic reticulum. *Eur J Biochem.* **1985**, *153*(3):451–7.

Suman, S. K.; Ravindra, D.; Sharma, Y.;Mishra, A. Association properties and unfolding of a βγ-crystallin domain of a Vibrio-specific protein. *PLoS One.* **2013**, *8*, e53610.

Sun, H.; Squier, T. C. Ordered and cooperative binding of opposing globular domains of calmodulin to the plasma membrane Ca-ATPase. *J Biol Chem.* **2000**, *275*(3):1731-8.

Sutton, R. B.; Davletov, B. A.; Berghuis, A. M.; Su¨dhof, T. C.; Sprang, S. R. Structure of the first C2 domain of synaptotagmin I: a novel Ca^{2+} phospholipid-binding fold. *Cell.* **1995**, *80*, 929-938.

Symth, J. T.; DeHaven, W. I.; et.al. Emerging perspectives in store-operated Ca^{2+} entry: Roles of Orai, STIM and TRP. *Biochim Biophys Acta.* **2006**, *1763*, 1147-1160.

Takemura, H.; Putney, J. W. Capacitative calcium entry in parotid acinar cells. *The Biochemical Journal.* **1989**, *258* (2), 409-12.

Tang, S.; Mikala, G.; Bahinski, A.; Yatani, A.; Varadi, G.; Schwartz, A. Molecular localization of ion selectivity sites within the pore of a human L-type cardiac calcium channel. *J. Biol. Chem.* **1993**, *268*,13026-13029.

Taylor, C. W.; Prole, D. L.; Rahman, T. Ca^{2+} Channels on the Move. *Biochemistry.* **2009**, *48*, 12062-12080.

Uversky, V. N.; Winter, S.; Lober, G. Use of fluorescence decay times of 8-ANS-protein complexes to study the conformational transitions in proteins which unfold through the molten globule state. *Biophys Chem*. **1996**, *60*(3):79-88.

Vig, M.; Beck, A.; Billingsley, J. M.; Lis, A.; Parvez, S.; Peinelt, C.; et al. CRACM1 multimers form the ion-selective pore of the CRAC channel. *Curr Biol.* **2006a**, *16*, 2073-9.

Vig, M.; Peinelt, C.; Beck, A.; Koomoa, D. L.; Rabah, D.; Koblan-Huberson, M.; et al. CRACM1 is a plasma membrane protein essential for store-operated Ca^{2+} entry. *Science* **2006b**, *312*, 1220-3.

Vig, M.; DeHaven, W.I.; Bird, G.S.; Billingsley, J.M.; Wang, H.; Rao, P.E.; Hutchings, A.B.; Jouvin, M.H.; Putney, J.W.; Kinet, J.P. Defective mast cell effector functions in mice lacking the CRACM1 pore subunit of store operated calcium release-activated calcium channels. *Nat. Immunol.* **2008**, *9*, 89–96.

Vig, M.; Kinet, J. P. Calcium signaling in immune cells. *Nat Immunol.* **2009**, *10*, 21–7.

Wei, C. C.; Motl, N.; Levek, K.; Chen, L. Q.; Yang, Y. P.; Johnson, T.; et al. Conformational States and kinetics of the calcium binding domain of NADPH oxidase 5. *Open Biochem J.* **2010**, *4*, 59–67.

Wenk, M.; Jaenicke, R. Calorimetric analysis of the Ca^{2+}-binding βγ-crystallin homolog protein S from *Myxococcus xanthus*: intrinsic stability and mutual stabilization of domains. *J. Mol. Biol.* **1999**, *293*, 117–124.

Wolfe, P. C.; Chang, E. Y.; Rivera, J.; Fewtrell, C. Differential effects of the protein kinase C activator phorbol12- myristate13-acetate on calcium responses and secretion in adherent and suspended RBL-2H3 mucosal mast cells. *J. Biol.Chem.* **1996**, *271*, 6658-6665.

Wu, M. M.; Buchanan, J.; Luik, R. M.; Lewis, R. S. Ca^{2+} store depletion causes STIM1 to accumulate in ER regions closely associated with the plasma membrane. *J. Cell Biol.* **2006**, 174, 803–813.

Yamniuk, A. P.; Ishida, H.; Lippert, D.; Vogel, H. J. Thermodynamic effects of noncoded and coded methionine substitutions in calmodulin. *Biophys J.* **2009**, *96*(4):1495-507.

Yang, J.; Ellinor, P. T.; Sather, W. A.; Zhang, J. F.; Tsien, R. W. Molecular determinants of Ca^{2+} selectivity and ion permeation in L-type Ca^{2+} channels. *Nature.* **1993**, *366*, 158-161.

Yang, W.; Lee, H. W.; Hellinga, H.; and Yang, J. J. Structural analysis, identification, and design of calcium-binding sites in proteins. *Proteins.* **2002**, *47*, 344-356

Yap, K. L.; Kim, J.; Truong, K.; Sherman, M.; Yuan, T.; Ikura, M. Calmodulin target database. *J Struct Funct Genomics.* **2000**, *1*(1):8-14.

Ye, Q.; Li, X.; Wong, A.; Wei, Q.; Jia, Z. Structure of calmodulin bound to a calcineurin peptide: a new way of making an old binding mode. *Biochemistry*. **2006**, *45*, 738-745.

Ye, Q.; Whang, H.; Zheng, J.; Wei, Q.; Jia, Z. The complex structure of calmodulin bound to a calcineurin peptide. *Proteins*. **2008**, *73*, 19-27.

Yeromin, A. V.; Zhang, S. L.; Jiang, W.; Yu, Y.; Safrina, O.; Cahalan, M. D. Molecular identification of the CRAC channel by altered ion selectivity in a mutant of Orai. *Nature*. **2006**, *443*, 226-229.

Yuan, J. P.; Zeng, W.; Dorwart, M. R.; Choi, Y-J.; Worley, P. F.; Muallem, S. SOAR and the polybasic STIM1 domains gate and regulate Orai channels. *Nature Cell Biology*. **2009**, *11*, 3.

Zhang, S. L.; Yeromin, A. V.; Hu, J.; Amcheslavsky, A.; Zheng, H.; Cahalan, M. D. Mutations in Orai1 transmembrane segment 1 cause STIM1-independent activation of Orai1 channels at glycine 98 and channel closure at arginine 91. *PNAS*. **2011**, *108*(43):17838-43.

Zuehlke, R. D.; Pitt, G. S.; Deisseroth, K.; Tsien, R. W.; Reuter, H. Calmodulin supports both inactivation and facilitation of L-type calcium channels. *Nature.* **1999**, *399*,159-162.